THREE DIMENSIONAL MEASUREMENT BASED ON THEODOLITE-CCD CAMERAS

by

YI DONG HUANG

A thesis
submitted for the degree of
Doctor of Philosophy
of the
University of London

Department of Photogrammetry and Surveying
University College London
Gower Street
London WC1E 6BT
United Kingdom

1993

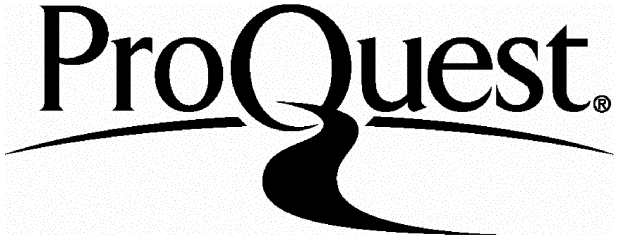

To Xiaojuan

THREE DIMENSIONAL MEASUREMENT BASED ON THEODOLITE-CCD CAMERAS

Abstract

This thesis concerns the investigation of the fundamental problems of three dimensional measurement using the theodolite-CCD camera, which is formed by attaching a CCD camera rigidly to the telescope of a theodolite.

A novel method - the camera-on-theodolite method - is proposed for the calibration of the theodolite-CCD camera. This method is also applicable to the calibration of any other cameras that can be mounted on the telescope of a theodolite. The most significant advantage of this method over previous ones is the dispensability of control target fields. The effectiveness of the method is proved with both simulation and experiments. Computer software is produced for implementing the new method in routine CCD camera calibration and is proved by experiments to be efficient.

Algorithms are designed and computer programs produced for automatic location of circular target images to subpixel accuracy. The algorithms involve parabolic interpolation of gradients at edge points of target images followed by least squares fitting of the edges with ellipse. The accuracy of target image location achieved by the algorithms is assessed using three methods developed by the author and is found to be as high as 1/50 pixel.

One of the most important measuring functions of theodolite-CCD cameras - theodolite scanning photogrammetry - is investigated in which a long focus lens is used to take images at large scale serially in grid form to cover the measured object. It is shown with experiments that this function can either improve the accuracy of CCD cameras in object coordinate determination for a specified object coverage or increase the object coverage of the CCD cameras for a specified accuracy in object coordinate determination.

Contents

Acknowledgement

I would like to thank my supervisor Professor Ian Harley, who has made considerable contributions to the research and the thesis. It is he who pointed out a mistake in the drafted mathematic derivation and also he who has corrected countless miswordings in the manuscript of the thesis. Without his contributions, the thesis would not have been completed.

I would also like to thank other members of staff in the Department of Photogrammetry and Surveying who have helped me one way or another during the course of the research. Specifically, I would like to thank Mr David Chapman who has helped fix the CCD camera into the damaged Kern EDM mount, Dr Arthur Allan who triggered the idea of making paper targets with Macintosh computers and Laser printers, Mr Philip Eales who introduced me to use of PCVision and Vicar image processing system, Mr James Pearson who diagnosed the problems in the theodolite computer communication, Mr Keith Atkinson who taught me how to use the Wild P32 camera, and finally Professor Peter Muller who provided me with some helpful literature at the early stage of the research.

My thanks should also extend to Ms Andrea Murray, my program officer, and other relevant members of staff in the Department of Technology Cooperation of the British Council as well as those in the State Education Commission of China who ensured the funding for the period of the three year study.

Chapter 1. Introduction

With the advance of science and technology, more and more complicated measuring tasks are emerging on one hand, and on the other hand more and more sophisticated measuring tools and techniques become possible. This thesis is about the investigation of the technique of three dimensional measurement based on the combination of the state-of-the-art techniques from photogrammetry, surveying and digital image processing.

1.1 Outline of previous research

Photogrammetry has many well known advantages over other techniques in three dimensional measurement. Film-based conventional photogrammetry in practice is, however, still limited in that a long post processing period is needed and that the specific instruments are expensive in cost and maintenance. Recent researches in photogrammetry have, therefore, been focusing on eliminating these limitations by extensively introducing computer technology to realize automatic, digital or real-time measurement. A few existing systems, which are representative in the digital context in the author's view, are selected to discuss below to show the current status of research and the problems left to solve.

MAPVISION: (Haggrén, 1987) This is to the author's knowledge the earliest commercially available photogrammetric system using CCD cameras and digital processing which can be found in the photogrammetric literature. Its prototype was

first published in 1985 and a new version became operational in 1986 (Haggrén, 1986). This system consists of four CCD cameras as standard and can be extended to include eight cameras. Each of the CCD cameras is digitized to 512 × 512 8-bit pixels. The host computer is an Intel SYS 310-17C with 8Mhz 80286 CPU and 80287 NDP. When in operation, the system is first set up and calibrated using 15-25 control points with known three dimensional coordinates. The DLT algorithm is then used to determine all the orientation parameters including lens distortion parameters. Although theodolite triangulation is used to coordinate the control points, the whole calibration phase is reported to take only less than one hour for an object 5 metres in size. In the measuring phase, a laser beam is projected onto the object to form a circular spot. The spot is recognised on each image by subtracting the image without the spot from the image with the spot. The spot image is then located using the original grey level information to an accuracy of 0.05 pixels. The spot image coordinates of all the images are finally used, together with the predetermined orientation parameters, to intersect the three dimensional coordinates. The accuracy is reported to reach 1/10,000 of the object size. The measuring time for one point is 1.5-2.7 second.

The principal advantages of Mapvision are that it provides an on-line three dimensional determination of any specified points within quite a large field of view and depth of field with a high accuracy and that the hardware configuration is simple and flexible, without needing any precise mechanical or optical parts. Some straightforward

improvements on the system are possible such as incorporating bundle adjustment in order to reduce or even avoid the use of control points, producing software for multiple target identification in certain cases and speeding up the whole system by upgrading the host computer. Some of the improvements had in fact been done by the time of last ISPRS Commission V symposium in Zürich.

Other similar systems have also been reported. VICON was presented by Oxford Metrics Ltd. in Oxford in 1984 for dynamic three dimensional measurement and analysis using attached retroreflective targets (Whittle et al, 1985 and Macleod et al, 1990). It has been commercially available for long and been successfully applied in the measurement of human movement. El-Hakim presented an "optical CMM" (El-Hakim and Barakat, 1989) where, as in a mechanical CMM, a pointing probe is used instead of a laser beam for measuring inside a complicated machine part. This system was also designed for pointwise measurement applications. Other research on optical CMM was reported by Schneider et al (1990) where multi-point measurement was possible. Neither of the latter two systems has been commercialised.

The accuracy of all the above mentioned systems is ultimately limited by the resolution of the CCD cameras. This is the main reason why conventional analogue photogrammetry has not yet been replaced in many very high accuracy industrial measurement applications.

The RSC (réseau scanning camera) system (Luhmann and

Wester-Ebbinghaus, 1987a, 1987b) is an example of effective efforts to extend the resolution of digital image sensors. In the RSC system, the whole format of the image is captured by shifting a standard CCD image sensor chip in the focal plane of the camera and capturing sub-images one by one. The correction of the geometric relationship among all the sub-images is carried out numerically with the help of a precise réseau plate which is fixed immediately in front of the focal plane. After CCD shifting, the whole format reaches a resolution of 5500×7050 sensor elements, which endows the system with an accuracy potential comparable to that of a large format film camera. Another remarkable innovation in RSC, which may also apply to other camera design, is that the sub-images can be focused individually to form sharp images all over the format without changing the interior orientation parameters of the camera. Moreover, the shifting of the CCD chip can be controlled with a joystick against a whole format viewfinder such that we can select for imaging only those patches of interest. The system normally uses bundle adjustment and self-calibration to determine three dimensional coordinates. Multiple, well defined targets, multiple stations, and convergent configuration are adopted to ensure the best accuracy.

The design of RSC shows an economical way to obtain high resolution images, which is undoubtedly very significant in consideration of the high price of the high resolution CCD cameras on the market. With RSC cameras, on-line digital photogrammetry may prove superior to film-based photogrammetry in both accuracy and cost. But, unfortunately, it cannot

capture data instantaneously, which means it is applicable only to fairly stable objects and environment. Many other problems, which are common to all high resolution digital photogrammetric systems, still remain to be solved before the RSC system comes into operational use. For example, a huge storage space and fast processing speed are required for the 21Mb image data generated per full image. Besides, the first experiment with the RSC system (Bösemann, et.al., 1990) has shown that the a posteriori accuracy of target image location with the RSC system is only half of that with the single standard CCD cameras. The cause was thought to be the poor accuracy of the réseau crosses and their image location, which is hopefully to be verified and overcome soon.

The Kern (Swiss) SPACE system (Gottwald, 1987,1989) is an automated three dimensional measuring system based on precise motorized theodolites with an integrated CCD image sensor. Theodolites are common angle-measuring instruments widely used in engineering surveying and geodesy. The integrated CCD image sensors in the theodolites in the SPACE system act as the eyes of a human operator, together with the servo-motors, to realise automatic aiming. The principle for three dimensional coordinate determination is essentially the same as the well known triangulation principle used in surveying and geodesy. In practice, the pseudo-photo principle and bundle adjustment originating from photogrammetry are adopted for a more convenient set up and orientation, which may be the main reason why this system has been more associated with people in the photogrammetric circle rather than those in the surveying circle.

Owing to the better than 1" of arc angle-measuring accuracy of the theodolites, the SPACE system is capable of determining three dimensional coordinates with an accuracy up to 1/200,000 of the object size (estimated for the case of dual head triangulation). The theodolites can rotate at a speed of up to 55°/sec and the system can measure 10 points per minute. One of the main working modes of the SPACE system is to measure the three dimensional coordinates of discrete target points automatically after being given or taught their approximate coordinates. This function is very useful in the periodical monitoring of the displacement and deformation of large structures frequently found in civil engineering and manufacturing industry. Another working mode of SPACE is to evaluate three dimensional surfaces by automatically measuring a dense pattern of points projected and scanned onto the object surface. For this purpose laser spot projectors are also provided by the manufacturer as accessories of SPACE. This function can provide range images for machine vision and three dimensional data input for CAD/CAM, which in turn serve a variety of purposes. The SPACE system can also be tailored flexibly and programmed by the user to cover specific measurement cases.

The SPACE system has a number of advantages compared with the other systems mentioned. It has no limitations in either the field of view or the depth of field. This character is to be significant when widely separated points are measured. Secondly, the SPACE system can take advantage of various orientation methods established in surveying to determine directly the relative and absolute orientation parameters

rather than relying on bundle adjustment which is unfavourable in some circumstances. Thirdly, when used for profiling or surface evaluation, the SPACE system can have one of its theodolites to act as a laser projector by feeding laser light into the telescope using the "laser eye piece" (Gottwald, 1989). Because of the high precision of the theodolite, the laser beam projected through the theodolite can act as a precise line for intersection with the line of sight from the other theodolite. This may be compared with the MAPVISION and the RSC systems where a separate laser projector with scanning mechanism may be needed which may not have sufficiently precise directivity to act as an intersection line itself.

Unfortunately, the SPACE system adopts pointwise recording and has an even lower recording speed than the RSC system where patch-wise recording is adopted. Again, the system must remain stable during the whole procedure of recording. In addition, because of the lack of an overview of the scene, the SPACE system requires rather detailed initial information or operator teach-in to be entered before it can carry out automatic measurement.

In summary of the review, the theodolite based measuring systems like the SPACE feature extremely high accuracy in individual pointing and an almost unlimited field of view but they can only measure objects point by point. The CCD based measuring systems like the MAPVISION and the RSC have a capability of instantaneous image recording but, comparatively, they cannot reach either as high an accuracy or as wide a field of view as theodolites can because of the

relatively low resolution of CCD cameras. The features of these two types of measuring systems complement each other and are surely preferred by different measurement projects. The point to which the author's attention was drawn during the conception stage of the project was that some elaborate combination of the theodolite based system and the CCD based system would make a better measuring system that might possesses all the features of the two put together and more.

1.2 Why theodolite-CCD cameras ?

The potential advantages

After having analyzed the previous research, the observation was made that attaching a CCD camera on each motorized theodolite of the SPACE system may improve the system and allow many more functions at only slight extra cost.

Attaching the CCD camera was conceived to be straight forward without interfering inside the theodolite, so that the additional cost is hoped to be not much more than the cost of the CCD camera. The attaching of the CCD camera was also conceived to be rigid so that the camera always rotates by the same angle as the telescope does both horizontally and vertically. In the combined instrument, the camera can still take images and the theodolite can still measure angles as usual.

It was envisaged that if the motorized theodolites in the SPACE system was modified as conceived above, it would acquire

many additional functions, among which were the following:

1) Theodolite scanning photogrammetry The CCD camera, rotatable together with the telescope of the theodolite, could be mounted with a long-focus lens to take images at a scale as large as required by the specified accuracy. The motorised theodolite on which the CCD camera was mounted would rotate as a scanning device so that the CCD camera could take a number of images to cover the whole object to be measured. The geometric relationships among all the images taken at the theodolite station could be determined through the theodolite readings after appropriate calibration and orientation. This feature would overcome the limitation of the low resolution of CCD cameras in three dimensional measurement.

2) Automated target searching for discrete point coordination While the system would still be used to coordinate discrete targets point by point with theodolite intersection, the CCD cameras could act as a pair of 'searching eyes' with wide-angle lenses. In principle, the scene would be first imaged by the pair of wide-angle cameras and the targets in the scene would then be detected and located roughly by photogrammetry. Finally, the rough three dimensional coordinates would be used to guide the telescopes to point at the targets individually for precise determination.

3) Automated direct orientation for real-time photogrammetry The system could be used as a pair of CCD cameras to capture images instantaneously for real-time photogrammetric work. In this case, both the relative and the absolute orientation

parameters of the cameras could easily be determined directly by means of the theodolites no matter how unfavourable the scene and the configuration were. This orientation procedure could also be automated.

4) Measuring while tracking With extensive development, the system would conceivably be capable of measuring the geometric status of a dynamic object while tracking it: that is to say, it might measure continuously in time the size, shape, angular velocity and acceleration of the object, as well as the position, velocity and the acceleration of its centroid. This function would result from the combination of motorized theodolites and CCD cameras and can scarcely be found in other systems.

Based on the above observations of the potential advantages of the combination of theodolite and CCD cameras, the research was motivated in the direction of the investigation of such combination for use in three dimensional measurement. The combined device is referred to as theodolite-CCD camera throughout the thesis.

1.3 The objectives of the research

Having set a direction for the research as such, how far it can go along this direction is inevitably affected by the resources and time allowed. Because neither a SPACE system nor a motorized theodolite was available, all of the above envisaged functions could not possibly be investigated. An ECDS system -the non-motorized version of the SPACE system,

was, however, available as well as an imaging system, which did make the investigation of some fundamental respects feasible.

The objectives of the research were therefore set as follows:

1) Calibration and orientation of theodolite-CCD cameras;
2) Automatic target image location to sub-pixel accuracy;
3) Accuracy test of three dimensional determination using the theodolite-CCD camera system in the mode of theodolite scanning photogrammetry.

Calibration, orientation and the automatic target image location are the fundamental problems that must be solved in order to make the theodolite-CCD camera system work. They are the prerequisite conditions that must be met before any advanced functions previously envisaged could possibly be developed in the future. The accuracy test of coordinate determination using theodolite scanning photogrammetry is important in that it would demonstrate one of the important advantages of theodolite-CCD camera system and add to the objective proof of the success of the techniques of calibration, orientation and image processing proposed in the thesis.

1.4 The contribution of the thesis

The most significant contribution of the research is the proposal of a novel camera calibration method -- the camera-on-theodolite method. This method needs no target array but

only two targets. It is applicable to any cameras mountable on the telescope of a theodolite although it is particularly suitable for a theodolite-CCD camera system. The method could be implemented fully automatically with a motorized theodolite like Wild TM-3000 or Kern E2-SE. Operational software has been produced by the author for using this method in the routine calibration of CCD cameras. The effectiveness and efficiency of the method and the software have been proved with both simulated and real experiments. These experiments as well as the principle of the method are presented in Chapter 3.

Algorithms have been designed and computer software produced to locate circular target images automatically to an accuracy of 1/50 pixel. These algorithms and software can also be applied to other digital photogrammetric research projects or applications where similar circular targets are used. Three methods have been devised and used to assess the accuracy of target image location. Computer programmes for conjugate target image correspondence which is necessary for three dimensional measurement have also been produced and used in experiments. These are the contents of Chapter 6.

Experiments have been carried out to test the accuracy of three dimensional measurement of the theodolite-CCD cameras when used in the mode of theodolite scanning photogrammetry. While the low spatial resolution of ordinary CCD cameras poses a serious problem in three dimensional measurement, insofar as one is unable to achieve both a high angular resolution and a wide field of view, the problem is overcome in scanning photogrammetry featured in theodolite-CCD cameras as here

proposed. The experiment results have shown that both high angular resolution and wide angular coverage are achievable. The principle of theodolite scanning photogrammetry for three dimensional measurement is described in Chapter 2, whereas the experiment details and results are reported in Chapter 7. It is noted that no similar experiments have been reported in the literature before although similar idea has been mentioned by Wester-Ebbinghaus (1988a).

Chapter 4 concerns system orientation, namely the exterior orientation of the theodolites comprising the three dimensional system. A number of methods established in surveying are introduced and commented on. The principle of using the mounted CCD cameras for theodolite orientation is also presented.

Chapter 5 describes the process of image acquisition using CCD cameras and image frame grabbers. The problem of linejitter is discussed.

Chapter 8 draws together the conclusions of the whole study and gives recommendation for future work.

All the computer programs used in this project were produced by the author except for the Vicar and Halo88 general image software bought with the PCVision image board and the Kern ECDS software.

Chapter 2. Three dimensional measurement based on theodolite-CCD cameras

2.1 The experimental theodolite-CCD camera

The theodolite-CCD camera is constructed by attaching a CCD camera rigidly on the telescope of a theodolite so that the camera and the telescope can rotate together about both the theodolite axes. The camera and the theodolite are optically independent of each other so that the camera can take images and the theodolite can still measure angles as usual, but both are connected to the host computer with image processor mounted.

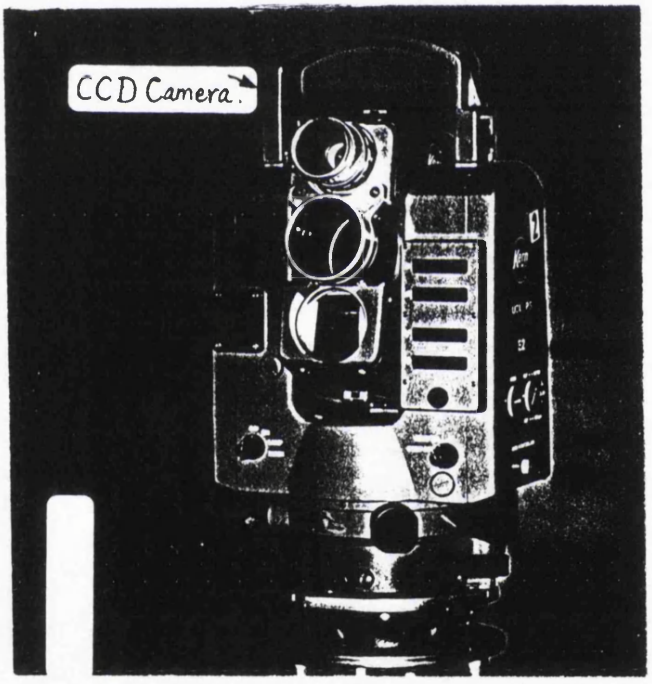

Picture 2-1 The experimental theodolite-CCD camera

The experimental theodolite-CCD camera for this research is shown in Picture 2-1. The theodolite is a Kern E2 one having 0.3" of arc angular positioning accuracy and a dual axial compensator. The flexible Philips CCD camera is fitted

into the moulded mount of a damaged Kern EDM, which is mountable on the telescope of the theodolite as designed to our satisfaction.

2.2 Definition of coordinate systems

The following coordinate systems and notations are defined. They are used consistently throughout the thesis. All the following coordinate systems are right-handed rectangular systems.

Camera coordinate system O_c-$x'y'z'$: O_c is the projective centre of camera. z' is perpendicular to the focal plane of the camera. x' (y') is perpendicular (parallel) to the *scanning line* direction of the image and increases with the number of line (sample). (Note that x and y are usually defined with fiducial marks in matric film cameras)

Two dimensional image coordinate system O_i-xy: x and y are parallel to x' and y' respectively. O_i is some convenient reference point, usually, the top-left corner of the images for CCD cameras (the intersection of the lines linking opposite fiducials for metric cameras). For a point in the image plane, the image coordinates and camera coordinates are related by the equation below.

$$\begin{pmatrix} x' \\ y' \\ z' \end{pmatrix} = \begin{pmatrix} x - x_0 \\ y - y_0 \\ -f \end{pmatrix} \qquad 2\text{-}1$$

x_o and y_o are the image coordinates of the principal point which is the point in which $O_c z'$ meets the focal plane. f is

the principal distance of the camera.

Telescope coordinate system O_t-XYZ: O_t is the rotational centre of the theodolite. X coincides with the tilt axis of the theodolite. Y coincides with the collimation axis and is positive as it points forward. The transformational relationship between this system and the camera coordinate system is denoted by the rotational matrix $\boldsymbol{R}_c$ and the translational vector $\boldsymbol{T}_c$ as below. They are determined by system calibration.

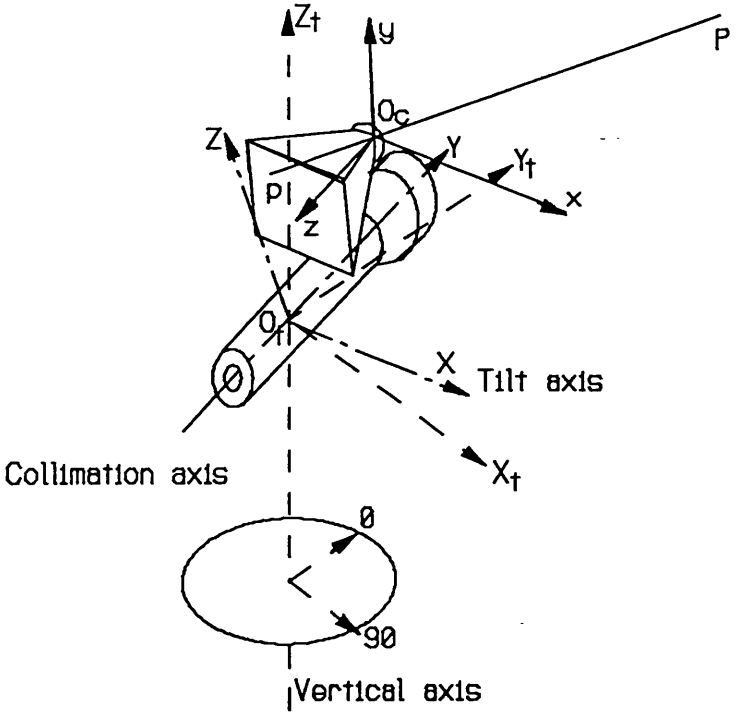

Fig.2-1 Definition of coordinate systems

$$\begin{pmatrix} X \\ Y \\ Z \end{pmatrix} = \boldsymbol{R}_c \begin{pmatrix} x' \\ y' \\ z' \end{pmatrix} + \boldsymbol{T}_c \qquad 2\text{-}2$$

$$\boldsymbol{R}_c{}^T \equiv \begin{pmatrix} a_{11} & a_{12} & a_{13} \\ a_{21} & a_{22} & a_{23} \\ a_{31} & a_{32} & a_{33} \end{pmatrix}, \quad \boldsymbol{T}_c \equiv \begin{pmatrix} t_x \\ t_y \\ t_z \end{pmatrix} \qquad 2\text{-}3$$

The rotational matrix is the function of three independent rotation angles. These three angles used in this thesis are ω, ϕ, κ as defined as that the reference (now the telescope)

coordinate system turns into a system parallel to the camera coordinate system by rotating about its X-axis by ω, then about its current Y-axis by ϕ and finally about its current Z-axis by κ. These three angles are defined as positive if they are counterclockwise when viewed from the positive ends of their respective axes. The expressions of the elements of the rotational matrix as functions of ω, ϕ, κ can be found in most of the photogrammetric text books (Wolf, 1983)

Theodolite coordinate system O_t-$X_tY_tZ_t$: O_t is the rotational centre of the theodolite. Z_t coincides with the vertical axis and points upwards. Y_t is parallel to some zero direction of the horizontal graduated circle. The relationship between this system and the telescope coordinate system is as follows:

$$\begin{pmatrix} X_t \\ Y_t \\ Z_t \end{pmatrix} = \boldsymbol{R} \begin{pmatrix} X \\ Y \\ Z \end{pmatrix} + \boldsymbol{T} \qquad 2\text{-}4$$

where obviously $\boldsymbol{T}\equiv\boldsymbol{0}$ and $\boldsymbol{R}$ is a function of the horizontal reading h and the vertical angle v of the theodolite:

$$\boldsymbol{R}^{\boldsymbol{T}}(h,v) = \begin{pmatrix} 1 & 0 & 0 \\ 0 & \cos v & \sin v \\ 0 & -\sin v & \cos v \end{pmatrix} \begin{pmatrix} \cos h & -\sin h & 0 \\ \sin h & \cos h & 0 \\ 0 & 0 & 1 \end{pmatrix}$$

$$= \begin{pmatrix} \cos h & -\sin h & 0 \\ \cos v \sin h & \cos v \cos h & \sin v \\ -\sin v \sin h & -\sin v \cos h & \cos v \end{pmatrix} \qquad 2\text{-}5$$

Object coordinate system O_w-$X_wY_wZ_w$: defined in accordance with the specification of a particular application. It is the

task of theodolite orientation to determine the relationship between the theodolite coordinate system and the object coordinate system, or to determine $\boldsymbol{R}_t$ and $\boldsymbol{T}_t$ in the following equation.

$$\begin{pmatrix} X_w \\ Y_w \\ Z_w \end{pmatrix} = \boldsymbol{R}_t \begin{pmatrix} X_t \\ Y_t \\ Z_t \end{pmatrix} + \boldsymbol{T}_t \qquad 2\text{-}6$$

$$\boldsymbol{R}_t{}^T \equiv \begin{pmatrix} m_{11} & m_{12} & m_{13} \\ m_{21} & m_{22} & m_{23} \\ m_{31} & m_{32} & m_{33} \end{pmatrix}, \qquad \boldsymbol{T}_t \equiv \begin{pmatrix} T_x \\ T_y \\ T_z \end{pmatrix} \qquad 2\text{-}7$$

2.3 The principle of three dimensional measurement using theodolite-CCD cameras

The theodolite-CCD camera system works on photogrammetric principles. As in photogrammetry, the CCD cameras in the system take two, to take the simplest case, overlapping images of the object to be measured. The image of the object is measured to get image coordinates. The process of orientation is also carried out to determine the position and orientation of the two cameras with respect to a certain three dimensional object coordinate system or to each other in the relative orientation cases. The space intersection algorithm is then used to derive the three dimensional coordinates of the object (points).

The characteristic of the theodolite-CCD camera system is that the orientation process is realized via the theodolites

in the system rather than through the cameras themselves using space resection or relative orientation as in the common photogrammetric practice.

The orientation process is tasked to determine the rotation matrix R_{cw} and the translation vector T_{cw} in the following transformation equation:

$$\begin{pmatrix} X_w \\ Y_w \\ Z_w \end{pmatrix} = R_{cw} \begin{pmatrix} x' \\ y' \\ z' \end{pmatrix} + T_{cw} \qquad 2\text{-}8$$

In the case of theodolite-CCD cameras, this transformation can be broken down into three steps of transformation whose parameters can be determined separately. By substituting in Eq.2-4 from Eq.2-2 and in Eq.2-6 from Eq.2-4, we obtain

$$R_{cw} = R_t \, R \, R_c \quad , \qquad 2\text{-}9$$

$$T_{cw} = R_t \, R \, T_c + T_t \qquad 2\text{-}10$$

· R_t and T_t are as defined in the previous section. They represent the transformation between the theodolite system and the object system. They are determined by theodolite observation in the process referred to as *theodolite orientation or system orientation*, which is described in Chapter 4;

· R_c and T_c represent the transformation between the camera system and the telescope system. They are determined together with the camera interior parameters by the process referred to as *system calibration* described in Chapter 3;

· R represents the transformation between the telescope

system and the theodolite system. It is the function of theodolite angular readings only, as stated in Eq.2-5.

It can be seen that after system calibration and system orientation have been completed, the orientation parameters of the cameras with respect to the object coordinate system can be found using Eq.2-9 and Eq.2-10. It is, therefore, possible to use the space intersection algorithm to calculate the three dimensional coordinates of object points.

2.4 Theodolite scanning photogrammetry

One of the most important advantages of the above orientation principle is that once the calibration and orientation of the system have been completed, the orientation parameters of the cameras, wherever they are now pointing, can be found from the current theodolite angular readings. If the camera is rotated to a new direction together with the telescope, only the new theodolite angle readings are needed to calculate the new orientation parameters. This advantage lends itself to the following measuring mode.

Theodolite scanning photogrammetry -- the CCD camera, rotatable together with the telescope of the theodolite, is mounted with a long-focus lens to take images at a scale as large as is required in order to meet the specified accuracy. The telescope of the theodolite on which the CCD camera is mounted rotates, as a scanning device, horizontally and vertically so that the CCD camera can take as many images as required to cover the whole object to be measured. The

orientation parameters of all the images taken at the theodolite station can easily be determined through the theodolite angle readings recorded at the time the images are taken. Figure 2-2 is a schematic diagram of 3 × 3 theodolite scanning photogrammetry (containing three times three frames of image) for measuring a three dimensional target array.

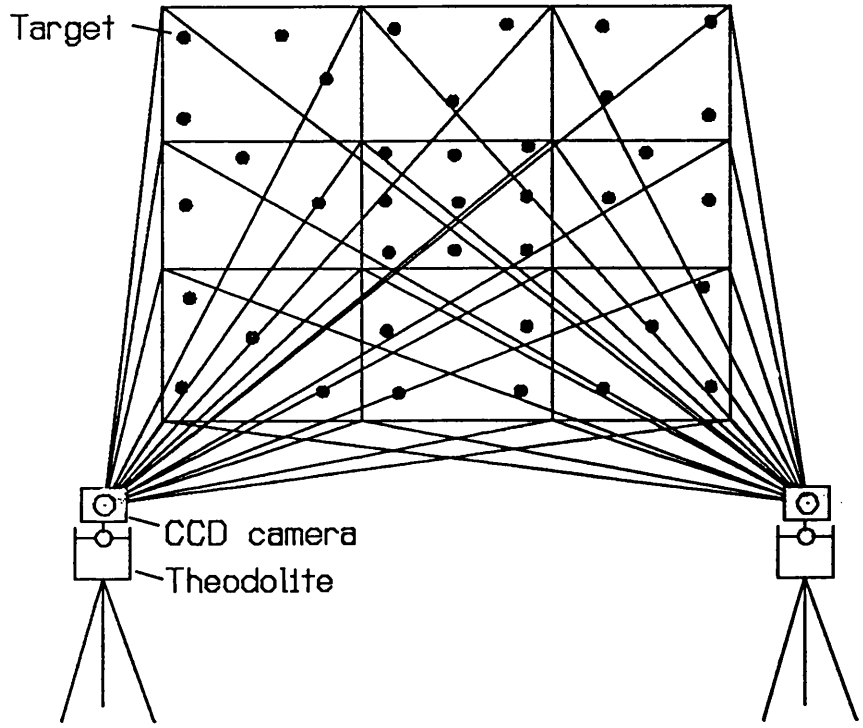

Fig. 2-2 3 x 3 theodolite scanning photogrammetry

Because of the low resolution of the affordable CCD cameras, on-line digital photogrammetry still has insufficient accuracy to replace film based photogrammetry. If these low resolution CCD cameras are made to achieve high enough accuracy by use of long focus lenses, the angular coverage must be reduced to a extent that practical application is very limited. With theodolite scanning photogrammetry, this problem can be overcome; both high object accuracy and wide object coverage can be achieved. In principle, the angular accuracy

and angular field of view of a theodolite-CCD camera working in the mode of theodolite scanning photogrammetry can match those of the theodolite itself.

Chapter 3. System calibration
- The camera-on-theodolite method

The system calibration involves the determination of the interior parameters of the CCD camera and the geometric relationship between the CCD camera and the theodolite which comprise the theodolite-CCD camera. The interior parameters of the CCD camera include the principal distance, the principal point coordinates and image distortion parameters (as shown in Eq.3-6). The geometric relationship between the camera and the theodolite is stated by three rotational and three translational parameters ie. R_c and T_c in Eq.2-2.

A new method - the camera-on-theodolite calibration method, is proposed for this purpose in this chapter. This method can determine the camera-theodolite parameters as well as the camera interior parameters. It can also be used as a general camera calibration method where only the camera parameters are of concern. Its most significant advantage over other methods is that it needs no control fields but only one or two targets. In the following, the method is proposed as a general camera calibration method.

3.1 Principle of the camera-on-theodolite method

3.1.1 The mathematical principle

Suppose that the camera to be calibrated is rigidly attached on the telescope of a theodolite so that it can rotate together with the telescope about both theodolite axes

horizontally and vertically. The camera coordinate system, telescope coordinate system and the theodolite coordinate system are defined as in Chapter 2 and are shown in Fig.2-1. With the telescope coordinate system as the reference system, an object point P, imaged as p, then leads to the collinearity equations below.

$$x - x_0 = -f \frac{a_{11}(X-r_x) + a_{12}(Y-r_y) + a_{13}(Z-r_z)}{a_{31}(X-r_x) + a_{32}(Y-r_y) + a_{33}(Z-r_z)} \qquad 3\text{-}1a$$

$$y - y_0 = -f \frac{a_{21}(X-r_x) + a_{22}(Y-r_y) + a_{23}(Z-r_z)}{a_{31}(X-r_x) + a_{32}(Y-r_y) + a_{33}(Z-r_z)} \qquad 3\text{-}1b$$

The telescope coordinates of point P again have a relationship with its theodolite coordinates as follows:

$$\boldsymbol{X} = \boldsymbol{R}^T(h, v)\ \boldsymbol{X}_t \qquad 3\text{-}2$$

where $\boldsymbol{R}(h, v)$ is a 3×3 matrix as stated in Eq.2-5, whose elements are functions of the current horizontal angular reading h and the vertical angle v of the theodolite (note that h is measured clockwise).

An important fact can be seen from Eq.3-1 and Eq.3-2, namely, that different image points can be obtained from the same object point P by rotating the telescope, and that the telescope coordinates of point P corresponding to different image points can be determined from the theodolite readings if the theodolite coordinates $\boldsymbol{X}_t$ of point P are known. As to $\boldsymbol{X}_t$, they are constant once the theodolite and the target P have been set up. They can be determined by initially sighting the

telescope at the target, recording the theodolite readings h_o, v_o and measuring the distance from the theodolite to the target D. The telescope coordinates of the target P at the time it is sighted are as

$$\boldsymbol{X}_0 = (\ 0\ D\ 0\ )^T \qquad 3\text{-}3$$

Substituting $\boldsymbol{X}_o$, h_o, *and* v_o into Eq.3-2, we have

$$\boldsymbol{X}_t = \boldsymbol{R}(h_0, v_0)\ \boldsymbol{X}_0 \qquad 3\text{-}4$$

Substituting the above into Eq.3-2 again we then obtain the following formula for computing the telescope coordinates.

$$\boldsymbol{X} = \boldsymbol{R}^T(h, v)\boldsymbol{R}(h_0, v_0)\boldsymbol{X}_0 = D\begin{pmatrix} -\cos v_0 \sin(h-h_0) \\ \sin v \sin v_0 + \cos v \cos v_0 \cos(h-h_0) \\ \cos v \sin v_0 - \sin v \cos v_0 \cos(h-h_0) \end{pmatrix} \qquad 3\text{-}5$$

Thus, each time the telescope is rotated to a new position, a new image point is formed and the coordinates of the corresponding object point referred to the telescope coordinate system may be found using Eq.3-5. After a set of image points have been formed and their telescope coordinates computed, any conventional algorithm can be applied to solve for the unknown interior camera parameters and exterior parameters with respect to the telescope coordinate system.

3.1.2 The case of a single target

If only one object point is used for calibration as described above, the method is equivalent to imaging a group

of control points situated on a spherical surface centred at the theodolite and with the distance to the target as its radius as shown in Fig.3-1(left). These equivalent control points are thus not coplanar. They should therefore theoretically give a unique determination of all the parameters present in Eq.3-1. However, the depth of scene these equivalent control points cover is very limited:

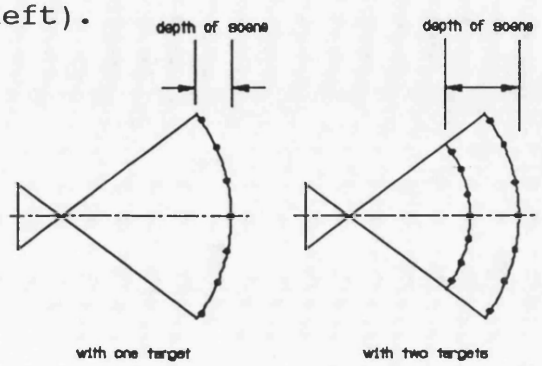

Fig. 3-1 The depth of scene

relative depth of scene = 1 - cos(half lens field angle)

Hence the depth for normal angle cameras (40°) is about 6% and that for wide angle cameras (50°) is 10%. It is unlikely that every parameter can be determined accurately in this condition. But it is predictably (though remaining to be proved) no worse than some calibration methods using coplanar control arrays, some of which, such as the Tsai's two-stage method (Tsai, 1985), have been reported effective.

3.1.3 The case of two targets

The value of this method in practice lies in the use of two targets. As illustrated in Fig.3-1(right) the depth of scene can be increased to any desired extent in this way. In this case, the two targets are sighted initially, two distances D_1 and D_2 measured, and two set of equivalent control

points created using Eq.3-5, which lie on two concentric spherical surfaces.

3.1.4 The determinability of the calibrated parameters

Assume $\omega=90°$, $\phi=0°$, $\kappa=0°$ (see Chapter 2 for the definition of ω, ϕ, κ.), which is likely to be the ideal case of mounting. Substituting X,Y,Z in Eq.3-1 with Eq.3-5, we have the following derivations*:

$$\delta x = \delta x_0 - \frac{xy}{f}\delta\omega + (f+\frac{x^2}{f})\delta\phi + y\delta\kappa + \frac{f}{N}\delta r_x - \frac{x}{N}\delta r_y + \frac{x}{f}\delta f + \frac{xr_y - fr_x}{DN}\delta D$$

$$\delta y = \delta y_0 - (f+\frac{y^2}{f})\delta\omega + \frac{xy}{f}\delta\phi - x\delta\kappa + \frac{f}{N}\delta r_z - \frac{y}{N}\delta r_y + \frac{y}{f}\delta f + \frac{yr_y - fr_z}{DN}\delta D$$

where $N = -(Y-r_y)$.

---

* The full derivation is rather tedious. The general expressions of the partial derivatives are, however, given in many photogrammetric text books (Wolf, 1983). We only need to substitute in those expressions with $\omega=90°$, $\phi=0°$, $\kappa=0°$ or $a_{11}=1$, $a_{23}=1$, $a_{32}=-1$ and a_{ij}(the remaining six)$=0$. Terms of δD are derived in the following for their speciality.

$$\frac{\partial x}{\partial D} = \frac{\partial x}{\partial X}\frac{\partial X}{\partial D} + \frac{\partial x}{\partial Y}\frac{\partial Y}{\partial D} + \frac{\partial x}{\partial Z}\frac{\partial Z}{\partial D} = -\frac{\partial x}{\partial r_x}\frac{\partial X}{\partial D} - \frac{\partial x}{\partial r_y}\frac{\partial Y}{\partial D} - \frac{\partial x}{\partial r_z}\frac{\partial Z}{\partial D}$$

$$= \left(-\frac{f}{N}\right)\left(\frac{X}{D}\right) + \left(\frac{x}{N}\right)\left(\frac{Y}{D}\right) + 0 = \left[-\frac{f(X-r_x)}{ND} - \frac{fr_x}{ND}\right] + \left[\frac{x(Y-r_y)}{ND} + \frac{xr_y}{ND}\right]$$

$$= \left[\frac{x}{D} - \frac{fr_x}{ND}\right] + \left[-\frac{x}{D} + \frac{xr_y}{ND}\right] = \frac{xr_y - fr_x}{DN} .$$

$\partial y/\partial D$ is derived in a similar way.

From these derivatives we can analyze the determinability of the unknown parameters qualitatively as follows:

1) The correlations between r_x and x_0, r_z and y_0, and r_y and f increase with the decrease of the depth of scene. Hence a large depth of scene is crucial to the accurate determination

of those parameters. It can be obtained without difficulty by using two targets.

2) D is completely correlated with r_x, r_y *and* r_z. They, therefore, cannot be determined simultaneously in the system.

3) Point 2 also implies that quite a large part of the error in the distance can be compensated for in the parameters r_x, r_y *and* r_z. Accurate measurement of D is necessary only when r_x, r_y *and* r_z are required from the calibration. In order to determine r, we need to measure D only with a relative accuracy of the level required for r, which is not difficult since D is large relative to r. This point also indicates that setting the objective centre of the camera near the centre of the theodolite is beneficial. Finding r_x, r_y *and* r_z is usually not required in conventional camera calibration.

3.1.5 Data reduction in analytical camera calibration

There are a number of well established data reduction methods for analytical camera calibration. They differ mainly in the way of formulating the relationship between the image points and their corresponding object points. The most well known ones in photogrammetry are the collinearity method and the DLT method (Abdel Azizi et.al., 1971). They are already very well covered in the photogrammetric literature. Some other calibration methods are also seen in the recent literature of computer vision. Those methods are slightly different in that they are more dedicated to solving for exterior parameters and basic interior parameters together on-

the-job in a non-iterative manner rather than for a complete set of lens distortion parameters as in photogrammetry.

The proposed camera-on-theodolite calibration method can use either the collinearity method or the DLT method for data reduction. They are very similar. The collinearity method features in solving directly for the original orientation parameters which have explicit geometric meanings, but needs initial estimates of all the unknowns and an iterative process. The DLT method can accept very coarse initial estimates of the unknowns and a linear solution is usually possible if only the first radial lens distortion parameter is adopted.

The camera-on-theodolite calibration method can also use the two-stage method for data reduction. This method was proposed by R. Tsai (1985) in the line of computer vision in order to enable the determination of both the orientation parameters and the radial lens distortion parameters without resorting to large scale nonlinear solution.

In the first stage of the method, a parallelism constraint, namely, that the vector from image origin to image point is always parallel to the vector to the corresponding object point normal to the optical axis, is used, which holds true whatever the radial distortion is. This constraint can be formulated by some linear equations with five or seven parameters which represent implicitly most of the orientation parameters but none of the distortion parameters. These parameters are solved for simply by linear solution and the

implicit orientation parameters are then determined uniquely. In the second stage, the collinearity equations are recalled with all the parameters appearing in the first stage as knowns and the lens distortion parameters and the rest orientation parameters that are not included in the first stage as unknowns. Only a small scale nonlinear solution is now needed to solve for the four or five parameters. This method is reported to take less computer time and does not need initial values.

A rather different method - the plumb-line method (Brown, 1971; Fryer and Brown, 1986) can also be used with the camera-on-theodolite method. It employs the property of perspective projection that the images of straight lines are also straight lines if without lens distortion. This property holds regardless of the camera orientation. The method can, therefore, determine the lens distortion parameters separately from the other orientation parameters. Such a solution could be more accurate since the correlation among those two groups of parameters, which exists in other methods, is avoided here. With the camera-on-theodolite method, only one or two straight lines are needed in the object space, which is a simplification.

Although any of the data reduction methods mentioned above can be used with the camera-on-theodolite method, the collinearity method (space resection) was written in the computer program and used throughout this project. This program can incorporate with any combinations of additional parameters in the systematic error model as follows:

$$\delta x = x(k_1r^2+k_2r^4+k_3r^6) + p_1(2x^2+r^2) + 2p_2xy + Ay + \\ + a_1xy + a_2x^2 + a_3y^2 + a_4x^2y + a_5xy^2 \qquad 3\text{-}6a$$

$$\delta y = y(k_1r^2+k_2r^4+k_3r^6) + 2p_1xy + p_2(2y^2+r^2) + By + \\ + b_1xy + b_2x^2 + b_3y^2 + b_4x^2y + b_5xy^2 \qquad 3\text{-}6b$$

where r is the radial distance from the principal point. k_1,k_2,k_3 are the radial lens distortion parameters; p_1 and p_2 are the tangential lens distortion parameters (Brown 1971); A and B are the affine deformation parameters; a_i, b_i (i=1,...,5) are the parameters of the polynomial error model.

3.2 Comparative experiments with simulated data

A computer simulated experiment has been carried out in order to compare the results of the new method with those obtained by using a geometrically strong three dimensional control field array. The effect of target distance error on calibration was also investigated in the experiment. The values of the simulated parameters are as follows:

type of camera: Wild P32;
format of photos: 90 mm horizontal, 65 mm vertical;
principal distance: f=64 mm;
principal point: x_0=0, y_0=0;
camera position w.r.t. the telescope coordinate system of the theodolite:

$r_x = 0$, $r_y = -20$, $r_z = 100$ mm;

orientation angles: ω=90°, ϕ=0°, κ=0°.

In the case of using two targets, the target to theodolite distances were set to be D_1=6000mm and D_2=8000mm. There were 25 image points corresponding to each target evenly distributed on the image plane. With the above values of parameters given, calibration with the space resection algorithm has been carried out 16 times with different random errors of the normal distribution with a standard deviation of 3 microns. The standard errors of the calibrated parameters have been calculated both from the variance-covariance matrix and from the true errors. These are shown in Row 2 and Row 3 respectively in Table 3-1, where they are referred to as theoretical s.e. and estimated s.e. respectively, i.e.

$$theoretic\ s.e. = \sigma_0\sqrt{q}$$

$$estimated\ s.e. = \sqrt{\frac{\Sigma\Delta^2}{16}}$$

where σ_0 is the unit weight standard deviation; q is the corresponding diagonal element of the inverse matrix of the coefficient matrix of the normal equations; Δ is the true error of the estimate of the parameter in question.

In Row 1 of the table are the theoretical standard errors of the parameter values calibrated with a simulated three dimensional control field which consists of 58 target points well distributed on 6 spherical surfaces of radii ranging from 5500 mm to 11000 mm from the theodolite.

In Rows 4,5 and Rows 6,7 are given the estimated errors of the parameter values calibrated when distance errors of approximate magnitude D/1000, both like and unlike, were imposed in the two-target case.

Rows 8 and 9 show the theoretical standard errors for the calibration for the single target method with D = 8000 mm for exclusion and inclusion, respectively, of the radial lens distortion parameters k_1 *and* k_2 (in Eq.3-6) as unknowns.

Table 3-1 **Results of Comparative Experiments with Simulated Data**

Row No.	Cases		f (μ)	x_o (μ)	y_o (μ)	k_1 10^{-4}	k_2 10^{-10}
1	3-D control field,theor. s.e.		6	3	4	16.2*	0.79*
2	two targets	theoretic s.e.	7	4	4	-	-
3		estimated s.e.	5.9	2.9	5.9	9.7	0.37
4	two targets estimated s.e.	D_1+6mm, D_2+8mm	5.9	2.9	5.9	9.7	0.37
5		D_1-6mm, D_2-8mm	5.9	2.9	5.9	9.7	0.37
6		D_1+6mm, D_2-8mm	6.5	1.9	8.8	6.3	0.26
7		D_1-6mm, D_2+8mm	7.2	1.9	4.6	6.2	0.26
8	one target theor. s.e.	excluding k_1,k_2	15	7	7	-	-
9		including k_1,k_2	3769	6.0	46.	630*	5.14*

* -- True errors of estimated parameters.

It can be seen from the results of the experiments that

1) with the two target method, the main interior elements can be calibrated with an accuracy comparable to that achieved with a well-conditioned and accurate three dimensional control field;

2) errors of 1/1000 in the distance between the two targets have little effect on the accuracy of calibration in the experimental case, which is quite representative;

3) when the distance between the two targets is sufficiently accurate (<1/1000), errors in target-to-theodolite distance of 1/1000 are tolerable;

4) the single target method is not so good as the two target method in accuracy, and even worse when radial distortion parameters are included. This is because the week geometric configuration of the generated equivalent target field which has a relatively small depth of field.

3.3 On-line CCD camera calibration without control fields

The camera-on-theodolite calibration method can be applied as a general camera calibration method. Because CCD cameras are usually light, compact and easy to be mounted on a theodolite, this method is especially suitable for the calibration of CCD cameras. For the routine use of this method, standard procedures have been designed and software produced. The hardware requirement is for a theodolite (with the CCD camera rigidly mounted on the telescope), a computer with image board, a measuring tape and two circular targets. The procedures are illustrated by the flow chart in Fig.3-2. A sample of the camera calibration result produced by the software is shown in the Appendix.

1). Check the design and accuracy prediction. In the software the image points are designed to be distributed in grid form with an adjustable grid density, such as 5 × 5. In the interests of simplifying the image processing, the two targets are required to be approximately on a straight line with the theodolite though this is not necessary in principle. In this stage, the approximate orientation parameter values, the grid density, the target to theodolite distances and the a priori standard deviation of image coordinates are input. The simulation program is invoked to give estimates of the precision of all calibrated parameters. The spacing of the image point grid or the target distances are then adjusted, if necessary, until the accuracy requirement is met.

2). Set the targets according to the design. Measure and enter the distances between the targets and the theodolite.

3). Aim the theodolite at the targets precisely. Enter the horizontal and vertical angular readings.

4). Data recording. Sequentially rotate the telescope to each of the designed directions in accordance with the angular readings prompted on the screen or with the windows shown on the video monitor within which you should enclose the target images. Record a sub-image enclosing the targets and record the theodolite readings at the same time (if a motorized theodolite is used, it moves automatically and successively to each of these positions without human intervention and will record the angular settings immediately after having recorded the image.).

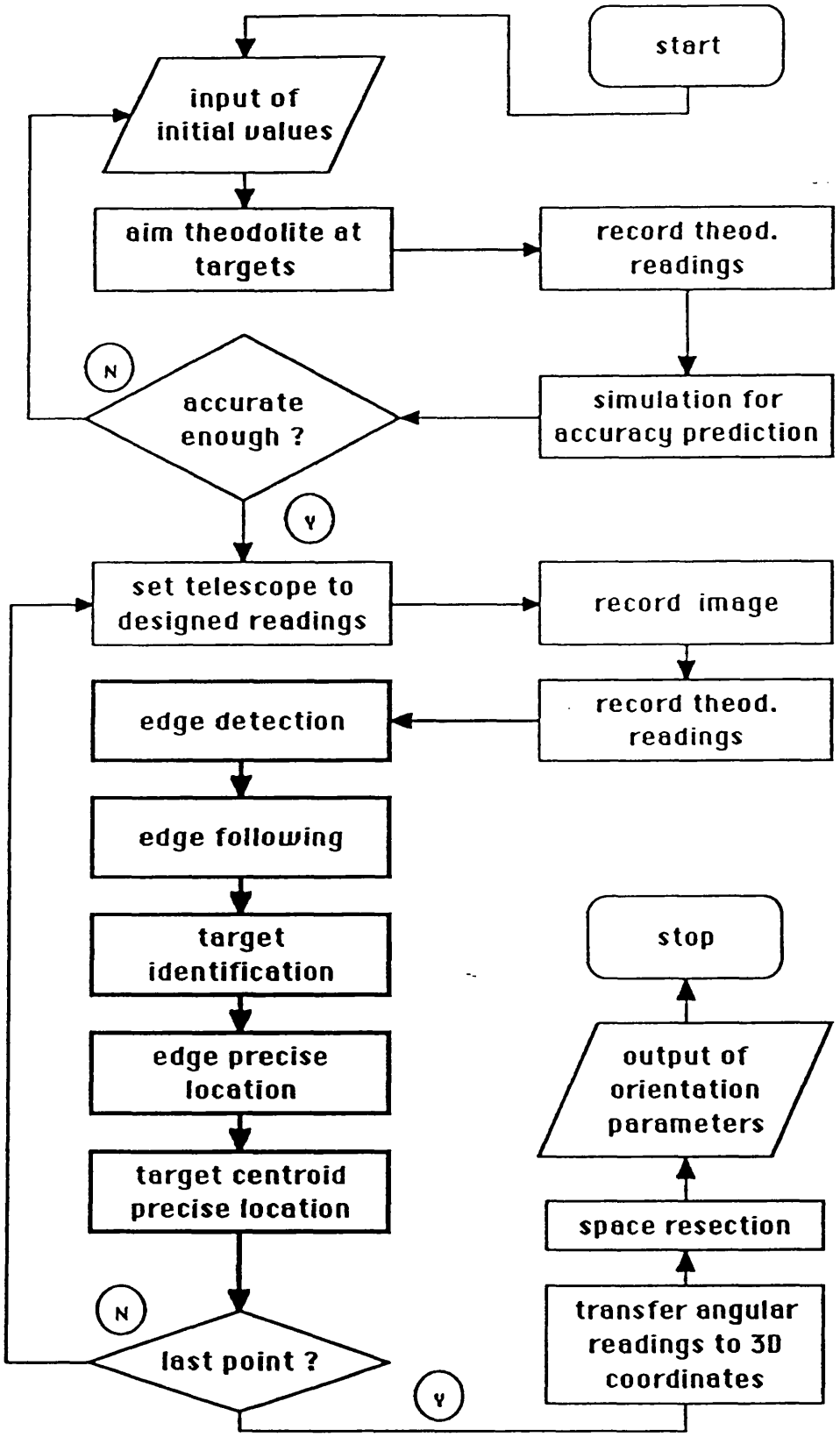

Fig. 3-2 Procedures of fast CCD camera calibration

5). Image processing. All the recorded sub-images are processed automatically by the computer as will be described in Chapter 6 in order to determine the coordinates of all the target images and to differentiate the near target from the far one.

6). Three dimensional coordinate calculation. Using Eq.3-5, calculate the three dimensional target coordinates corresponding to every target image using the recorded angular readings and the target-to-theodolite distances.

7). Space resection. Run the space resection and calibration program to determine the camera parameters. The calibration program can incorporate any combinations of the additional parameters in Eq.3-6.

3.4 Real experiments with a CCD camera

Using the software produced as described above, real experiments have been carried out with a CCD camera in order to test again the accuracy of calibration achieved by the new method and the new software.

The camera to be calibrated consisted of a Philips frame transfer CCD chip of a size of 4.5 mm × 6.0 mm with 588 × 604 cells. The video signal from the CCD camera was digitized by an IBM PC-XT computer and a PC-Vision Plus image board into digital images containing 480 × 512 8-bit pixels. The dimensions of a pixel were approximately 8.1 microns in x and 11.6 microns in y. Two lenses of different focal lengths were

experimented, one being 25 mm and the other being 51 mm. The theodolite used was the Kern E2 electronic one. The camera was fixed in an damaged Kern EDM mounting as shown in Picture 2-1. The targets were produced with MacDraw II on a Macintosh using a laserwriter printer.

The target-to-theodolite distances were measured with a tape to the nearest millimetre. The targets were sighted at three times both before and after the data recording stage in order to obtain precise values of h_o and v_o. Each angular reading was recorded to 0.1 mgon (0.3"). The collimation errors of the theodolite were found to be too small to require corrections; the stability and the repeatability of the system were found to be sufficiently good.

Two targets were used with the camera-on-theodolite method. 5 × 5 target images were generated from each target through theodolite rotation, which gave a total of 50 target images with corresponding three dimensional coordinates known. Some of the 50 target images were used for calibration while the rest used as check points for accuracy assessment. The accuracy of calibration was assessed by the root mean square of the residuals of back ray tracing which were the differences between the located image coordinates and those calculated with the three dimensional coordinates of the corresponding check points and the orientation parameters determined in the calibration. The calibration results and their accuracies are shown in Table 3-2 and Table 3-3 respectively. Three different combinations of additional parameters in Eq.3-6 were used respectively in the data

reduction of each calibration. They are denoted as

AP1: A and B only;

AP2: AP1 plus k_1;

AP3: AP2 plus $a_2, a_3, a_5, b_2, b_3, b_4$.

Table 3-2 **Values of calibrated parameters and their standard deviations in the real experiments**

		f pixel	x_0 pixel	y_0 pixel	k_1 10^{-12}	A 10^{-5}	B 10^{-3}
25 mm lens							
AP1	Values	2240.66	12.38	32.26		-0.565	0.381
	s.d.	0.71	3.76	2.50		0.157	0.00157
AP2	values	2242.96	21.46	43.76	0.308	-0.581	0.379
	s.d.	0.48	3.52	2.81	0.025	0.098	0.00099
AP3	values	2243.18	30.94	41.49	0.460	-0.607	0.375
	s.d.	0.60	6.56	3.24	0.083	0.121	0.00173
50 mm lens							
AP1	values	4678.65	7.80	40.09		-0.199	0.376
	s.d.	0.94	11.40	7.54		0.109	0.00109
AP2	values	4678.20	6.81	36.65	-0.028	-0.200	0.376
	s.d.	1.05	10.20	7.15	0.029	0.109	0.00111
AP3	values	4678.00	3.73	58.52	-0.058	-0.187	0.376
	s.d.	1.09	12.15	15.48	0.040	0.120	0.00182

* Note: the raw image coordinates needed to be shifted by 240 and scaled by 0.7 in x and shifted by 256 in y before using the calibration data.

It has been found from Table 3-2 that the values of the calibrated parameters are close to the specifications of the camera and therefore that no mistakes have been made in the

calibrations. The standard deviations are within reasonable ranges, which shows the viability of the method and the geometric configuration. The poor determination of the principal point shown by the large standard deviations was understood to be inevitable for such narrow angular fields of view associated with the camera, which were only 17° and 8° for the 25 mm and 51 mm lenses respectively.

Table 3-3 Accuracy of the CCD camera calibration in the real experiments (unit: pixel)

AP	25 mm lens						51 mm lens					
	RMS of residuals 32 control points			RMS error 18 check points			RMS of residuals 30 control points			RMS error 20 check points		
	σ_o	x	y	c	x	y	σ_o	x	y	c	x	y
AP1	0.090	0.042	0.108	0.080	0.050	0.101	0.061	0.032	0.071	0.063	0.035	0.082
AP2	0.053	0.032	0.059	0.057	0.036	0.072	0.061	0.031	0.071	0.064	0.035	0.083
AP3	0.040	0.022	0.043	0.065	0.023	0.089	0.060	0.025	0.066	0.068	0.028	0.092

σ_0 - standard error of unit weight a posteriori.
RMS_c - root mean square of RMS_x and RMS_y.

What is more important is the accuracy of calibration as shown in Table 3-3. The RMS of control point residuals in the AP3 row show that the precision of target image location is 0.02 to 0.03 pixel in x and 0.04 to 0.06 pixel in y, which coincides with that assessed by other methods to be described in chapter 6. The nearly equally small RMS errors of check

points indicate generally good modelling of the systematic errors by the parameters introduced, especially in the line (x) direction. These RMS errors from the check points are regarded as the measures of accuracy of the calibrations. As is shown in the table, the accuracy deteriorated in the sampling direction when the AP3 was introduced. This is understood to be caused by the line-jitter and the like which were not well modelled or impossible to model. Finally, it should be noted that the radial distortion parameter k_1 brought a significant accuracy improvement in the case with 25 mm lens although very little with the 51 mm lens.

The whole calibration procedure and software proposed here have been proved to be efficient and easy to handle. Only one operator was needed from beginning to end, except for the distance measurement. It took about thirty minutes for one run with 5×5×2 target images, out of which about ten minutes was spent on manually rotating the theodolite and entering the theodolite readings. If a motorized theodolite were to be used together with an upgraded PC computer, the total calibration time could be as little as five minutes.

3.5 Usability of the calibrated interior camera parameters

The accuracy of calibration assessed by check point ray back tracing only indicates the goodness of fitting between the bundle of rays defined by all the calibrated parameters and the check points used. It does not imply the accuracies of individual calibrated parameter values. Their theoretical

accuracies are measured by the standard deviations produced in the calibration solution. When a subset of the calibrated parameters are used in a later measuring task, it is the variance matrix of the subset of parameters and the way of using them that dictates the accuracy effect. Because the variance matrix is a non-diagonal one with covariances, its effect on a later measuring task is far from explicit.

It may be more useful to discuss this problem of usability in a particular context. Suppose that the camera-on-theodolite method is used as a general camera calibration method and that among all the calibrated parameters only the camera interior parameters are to be used in a later measuring application. They will be used directly as knowns and the space resection with a few control points will be carried out to determine the exterior orientation parameters in the application. This is a typical case of application and experiments have, therefore, been carried out for this case. The results are summarised in the Table 3-4.

In the experiments five independent sets of data were acquired through rotating the camera-theodolite with respect to two fixed targets as in the calibration process. The camera interior status was kept unchanged throughout the experiments and Data set 1 was used for calibration. The other data sets were used as later measuring tasks where the calibrated interior parameters were applied as knowns; some points were used for exterior orientation with space resection method, and some other points used as check points for ray back tracing.

Table 3-4 **Results of Experiments in the Usability of the Calibrated Parameters**

Data set	Number of control points for exterior orientation	Number of check points for back ray tracing	RMS error of check points (pixels)		
			c	x	y
1*	6	22	0.057	0.035	0.073
2	18	32	0.070	0.044	0.089
3	4	14	0.077	0.056	0.094
4	4	14	0.095	0.055	0.122
5	6	26	0.078	0.039	0.103

* Set 1 is that used for calibration; different points are used here for space resection and as check points. Only A,B,k_1 are applied as a.p..

After calibration with Data set 1, the standard deviations of the principal point coordinates were as large as 4 and 5 pixels, yet the accuracies of the results in the applications, as shown in Table 3-4 were all better than 0.06 pixel in x and 0.13 pixel in y. After allowing for the error of reorientation, these accuracies are very close to the accuracy of calibration assessed by the check point ray back tracing shown in Table 3-3 . This result may be explained as that the inaccuracies of the interior parameter values found in the calibration can be compensated for to some extent by the exterior orientation parameters to be determined later by

space resection in the assumed application. It is, therefore, shown that the calibrated interior parameter values may be used with confidence in other similar applications.

In the calibration of the proposed three dimensional measuring system using the camera-on-theodolite method, there does not exist the usability problem as discussed before because the system status is not changed between the calibration and later applications and all the calibrated parameters are used together in the later measuring applications. The accuracy assessed with check point ray back tracing can, therefore, be maintained in later measuring tasks.

3.6 Discussion

The camera-on-theodolite calibration method has been proved effective by both simulated and real experiments. The advantages of the method are summarised below.

1) There is no need to physically establish and measure a three dimensional array of control targets. Camera calibration can be performed for cameras of different formats and different focal lengths without the necessity of rebuilding a control array, or adapting its size, accuracy, density of points or the size of targets to the particular case.

2) The adaptability of the method lends itself to on-the-spot determination of the interior orientation (including lens

distortion) immediately before use of the camera; it also provides external orientation if it is required and if a few extra measurements are made with the theodolite.

3) Only one or two targets are used. All the target images, therefore, have uniform grey intensity and are of the same size, which are beneficial factors for accuracy.

4) The distribution of image points can easily be designed.

If the method is applied to a conventional film camera, the following disadvantages may be present:

1) Multi-exposure of a single target or a pair of targets in order to form enough image points may take considerable time.

2) A completely dark background may be required in order to expose all the target images on one single frame.

3) The installation of the camera onto the theodolite may become a problem if the camera is bulky.

When the method is used to calibrate a video (or CCD) camera, all the disadvantages listed above disappear. Many video cameras for vision use are small and compact and thus easy to mount on a theodolite. Multi-exposure on a video camera takes little more time. Different target images can be exposed onto different frames which share the same geometry.

The essence of this method is the creation of an

imaginary equivalent three dimensional solid from a simple feature through rotating the theodolite telescope which is defined as the three dimensional coordinate reference system with respect to which the camera is fixed in the course of calibration. Originating from this essence, some variations of the method are possible. For example, a plumb line or an any known straight line can be used to create any number of imaginary lines in various directions in the three dimensional space through theodolite rotation. A few targets arranged on a plumb line with measured interdistances may be used to create an imaginary cylinder by rotating the theodolite horizontally only in order to surmount the difficulty in vertical rotation encountered when the calibrated camera is too big (proposed by Ian Harley).

The full automation of CCD camera calibration using the camera-on-theodolite method is straightforward if a Leica motorized theodolite with automatic aiming function is used. The target to theodolite distance can be measured automatically with EDM or with two theodolite intersection in the case of on-the-spot calibration for subsequent dual-head three dimensional determination.

Chapter 4. System Orientation

The task of system orientation is to determine the relative geometric relationship among all the theodolite-CCD cameras (stations) which comprise the measuring system (relative orientation) and their spatial position and orientation in the reference object coordinate system chosen for a particular application (absolute orientation). Because the chosen reference object systems are often defined in a variety of forms, absolute orientation methods are more application dependent and better to be derived in practice. This chapter is then focused on the relative orientation.

4.1 Five-point orientation for non-levelled theodolites

The horizontal and vertical angular readings of a theodolite can be transferred into their corresponding rectangular coordinates of a pseudo photo if a focal length is assumed. That is the "pseudo-photo" principle of theodolite observations. By this principle we can transplant many methods and algorithms in photogrammetry into use for theodolites. Among these is the analytical relative orientation method for photograph pair, which can be used straightforwardly for the orientation between two theodolites.

The analytical relative orientation method is based on the coplanarity condition which states that the two rays (or lines of sight) from two theodolites to a common object point are coplanar with the base line that links the rotational centres of the two theodolites. An equation of coplanarity

condition can be formed for each observed object point (Wolf, 1983). Observing five points is necessary for the five relative orientation parameters. More points are needed to obtain a better accuracy and to allow blunder detection. A known distance between any two of those points or a measured base line is necessary for scaling.

4.2 Three-point orientation for levelled theodolites

For levelled theodolites the number of orientation parameters to be determined reduces from five to three. Thus only three points are necessary to be observed. As is seen, there is a trade-off between levelling the theodolites and observing two more points. If possible, the former is preferred for two reasons. The first is that modern electronic theodolites have precise self-correction devices for vertical axis inclination within some range. In these theodolites, the magnitude and the direction of the inclination of the vertical axis are determined and corrections added to each theodolite reading. The accuracy is believed to be higher than that of determination with five-point orientation method. The second reason is that levelling is one of the requirements which ensure a theodolite will work properly.

4.3 Theodolite orientation with reciprocal pointing

The relative orientation between two non-levelled theodolites can be fulfilled by pointing the theodolites at each other's centres and also at an object point. In principle, the scale factor is determined by measuring a

distance between one theodolite and the other or the object point. Kyle (1988) has described this type of methods in detail along with some reciprocal pointing methods.

Some other orientation schemes using reciprocal pointing exist: levelling theodolites and reciprocal pointing (with no object point); levelling theodolites, horizontal reciprocal pointing and pointing at one object point. The later is described in detail below because it is the method that was used in the experiments.

Define the reference object coordinate system O_w-$X_wY_wZ_w$ with the two theodolites involved so that the origin O_w is the rotational centre of the left theodolite, X_w axis is horizontal and pointing at the vertical axis of the right theodolite as positive, and Z_w axis is the vertical line through O_w and pointing upwards as shown in Fig.4-1. Level the theodolites. Point the theodolites at each other and take the horizontal angle readings α_l and α_r as shown in Fig.4-1. Point both the theodolites at an object point P and take the horizontal and vertical angles β_l, γ_l and β_r, γ_r respectively as shown in Fig.4-2.

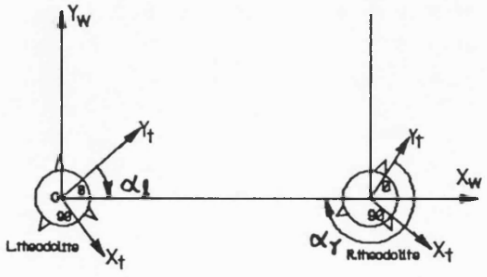

Fig.4-1 Reciprocal pointing

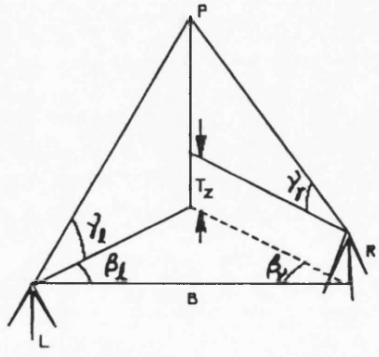

Fig.4-2 Pointing at an object point

From Fig.4-1 and Fig.4-2, the following expressions of the rotation matrices and translation vectors of the theodolites to the reference system can easily be derived.

$$\boldsymbol{R}_{t_l} = \begin{pmatrix} \sin\alpha_l & \cos\alpha_l & 0 \\ -\cos\alpha_l & \sin\alpha_l & 0 \\ 0 & 0 & 1 \end{pmatrix} \qquad 4\text{-}1$$

$$\boldsymbol{R}_{t_r} = \begin{pmatrix} -\sin\alpha_r & -\cos\alpha_r & 0 \\ \cos\alpha_r & -\sin\alpha_r & 0 \\ 0 & 0 & 1 \end{pmatrix} \qquad 4\text{-}2$$

$$\boldsymbol{T}_{t_l} = \boldsymbol{0} \ , \qquad 4\text{-}3$$

$$\boldsymbol{T}_{t_r} = \begin{pmatrix} B \\ 0 \\ \dfrac{B\ (\sin\beta_r\tan\gamma_l - \sin\beta_l\tan\gamma_r)}{\sin(\beta_l+\beta_r)} \end{pmatrix} \qquad 4\text{-}4$$

where B is the horizontal distance between the theodolites. According to the convention in photogrammetry, B is assumed of a provisional value during relative orientation. This value only affects the scale of the measured object (stereo model) but not the shape. The precise scale factor can be determined when B or a distance in the object space is measured precisely. This distance measurement can be carried out using various methods well established in geodetic surveying.

4.4 Theodolite orientation via the mounted CCD cameras

All the methods mentioned above use theodolite observation to fulfil orientation among theodolites. Alternatively, for a theodolite-CCD-camera system, we can also do the same thing through photogrammetry with the CCD cameras

which are mounted on the theodolites. In this method, instead of observing through theodolites, image coordinates are measured and the theodolite readings at exposure used. All the orientation parameters are written into the photogrammetric equations of condition as unknowns and solved for with the rigorous adjustment. This can take various formulations. In the following are derived two formulations with comments on their deviation from the standard collinearity equations. Although they were not used in the experiments, they may be useful in the future when multi-station large scale simultaneous solution is needed.

4.4.1 Collinearity equations with theodolite orientation parameters

Suppose that there is an object point P and that its corresponding image point is p. According to the collinearity principle the coordinates of these two points and the image projective centre O_c in the object coordinate system have the following relationship (see Chapter 2 for the notations):

$$\boldsymbol{X}_{w(P)} - \boldsymbol{X}_{w(O_c)} = s \left(\boldsymbol{X}_{w(p)} - \boldsymbol{X}_{w(O_c)} \right) \qquad 4\text{-}5$$

where s is a scale factor. Substituting from Eq.2-2 - Eq.2-7 the above equation turns to

$$\boldsymbol{R}_t^T \left(\boldsymbol{X}_w - \boldsymbol{T}_t \right) - \boldsymbol{R}\,\boldsymbol{T}_c = s\,\boldsymbol{R}\,\boldsymbol{R}_c\,\boldsymbol{x}' \qquad 4\text{-}6$$

where the subscripts P and p are omitted and $\boldsymbol{x}'$ are the camera coordinates as stated by Eq.2-1. Now, adopting the following notation

$$\begin{pmatrix} u \\ v \\ w \end{pmatrix} \equiv \boldsymbol{R}\,\boldsymbol{R}_c \begin{pmatrix} x-x_0 \\ y-y_0 \\ -f \end{pmatrix} \qquad 4\text{-}7$$

$$\boldsymbol{C} = (\ C_x \quad C_y \quad C_z\ )^T = \boldsymbol{R}\,\boldsymbol{T}_c \qquad 4\text{-}8$$

and eliminating s in Eq.4-6, we obtain the collinearity equations below,

$$\frac{u}{w} = \frac{m_{11}(X_w-T_x) + m_{12}(Y_w-T_y) + m_{13}(Z_w-T_z) - C_x}{m_{31}(X_w-T_x) + m_{32}(Y_w-T_y) + m_{33}(Z_w-T_z) - C_z} \qquad 4\text{-}9a$$

$$\frac{v}{w} = \frac{m_{21}(X_w-T_x) + m_{22}(Y_w-T_y) + m_{23}(Z_w-T_z) - C_y}{m_{31}(X_w-T_x) + m_{32}(Y_w-T_y) + m_{33}(Z_w-T_z) - C_z} \qquad 4\text{-}9b$$

It can be seen that by using these equations it is possible to solve for the orientation parameters $\boldsymbol{R}_t$ and $\boldsymbol{T}_t$ in a similar way to the analytical space resection or relative orientation when the theodolite readings at the time of image exposure are used as well as the image coordinates of the measured points.

Compared with the "Standard" collinearity formulation, the above equations have C terms in the fractions on the right hand sides. The left hand sides are the function of image coordinates and thus correlated. No established computer programs are known to be able to deal with this different form of equations without adaptation, even if the calibrated camera parameters are regarded as knowns and C terms as constants. New computer program, therefore, needs to be produced for the practical use of these equations. In addition, the accuracy of this solution for the orientation parameters is also yet to be investigated in the future. All these problems are interesting

but beyond the scope of the current project.

4.4.2 Keeping the standard form by introducing simple constraints

If we introduce intermediate parameters $\boldsymbol{X}_o = (X_o\ Y_o\ Z_o)^T$ Eq.4-6 breaks down into two groups as follows:

$$\boldsymbol{R}_t^T (\boldsymbol{X}_w - \boldsymbol{X}_0) = s\, \boldsymbol{R}\, \boldsymbol{R}_c\, \boldsymbol{x} \qquad 4\text{-}10$$

$$\boldsymbol{R}_t^T (\boldsymbol{T}_t - \boldsymbol{X}_0) = - \boldsymbol{R}\, \boldsymbol{T}_c \qquad 4\text{-}11$$

For each image point two equations can be formed from Eq.4-10 by eliminating s. For each image frame three equations can be written as Eq.4-11 for the three elements of $\boldsymbol{X}_o$. $\boldsymbol{R}_t$ and $\boldsymbol{T}_t$ are common for all image frames at each theodolite station. In order to use standard photogrammetric adjustment software like CAP, we could regard $\boldsymbol{T}_t$ as the coordinates of a pseudo object point and $-\boldsymbol{C}$ (or $-\boldsymbol{R}\boldsymbol{T}_c$) as the image coordinates of the corresponding image point. The pseudo object point is given the same name or number for all images at one station. Since $\boldsymbol{R}_t$ are identified as different for different frames of image by the software, although they are actually the same at a station, we still have to impose the following constraints for the rotational angles of $\boldsymbol{R}_t$:

$$\begin{aligned} \omega_k &= \omega_1 \\ \phi_k &= \phi_1 \qquad 4\text{-}12 \\ \kappa_k &= \kappa_1 \end{aligned}$$

where $k = 2,\ldots,n$, and n is the number of image frames. These

constraints are the variation to which the CAP needs to be adapted. This adaptation seems to be easier than that based on Eq.4-9. Unfortunately, even though CAP has been so adapted, this approach is still an approximate adjustment for two reasons. The first is that the entered observations are correlated and the software cannot take a non-diagonal covariance matrix of the observations. The second is that one condition is wasted for each image frame, which also means that at least two image frames have to be used to solve for the full orientation parameters. Whether all this approximation is tolerable or not is again yet to be investigated in the future.

Chapter 5. Digital image acquisition with CCD cameras

Most of the experiments carried out in this project involved the use of CCD cameras and frame grabbers for the acquisition of digital image. It is, therefore, necessary to briefly review here the working principles of these electronic imaging devices and to discuss their problems in photogrammetry. It should be noted that the ability to use these devices properly and the understanding of their principles and problems are crucial to the success of an author whose background is in photogrammetry in such a CCD oriented project as this. Of course CCD devices themselves are far from new in the discipline of electronic imaging.

5.1 CCD cameras

A CCD (charge couple device) array image sensor is an integrated array of MOS (metal oxide semiconductor) transistors. When biased with a voltage, each MOS element forms a potential well which is capable of collecting charges. When an image is focused on the array of MOS, electrons are knocked out of the atoms of the semiconductor and collected by the potential wells so as to form charge packets. The sizes of the charge packets are proportional to the local light intensities. If the electrodes for biases are arranged in a multiphase form and driven by multiphase clocks as is shown in Fig. 5-1, the signal charge packets will be shifted via the CCD itself to the output with the clocks.

In practice, there are mainly two kinds of structure with

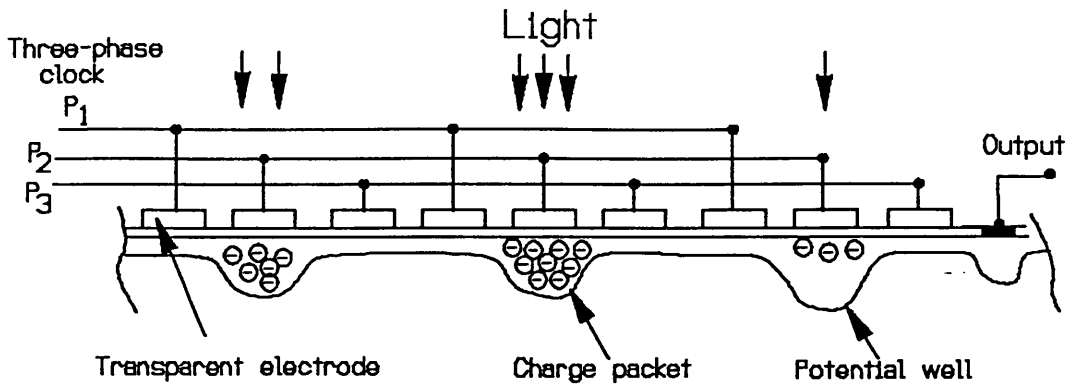

Fig. 5-1 Principle of CCD image sensors

respect to the way of charge transference. They are called frame transfer (FT) and interline transfer (ILT) and shown schematically in Fig.5-2 and Fig.5-3 respectively. In the FT the array is divided into an image section and a storage section. The storage section is of the same size as the image section but shielded from light and has the electrodes linked to different clocks. In operation, the electrodes of one phase (or the other two phases for the other field to achieve TV interlace) are held at high voltage to integrate charges in the image section. At the end of integration period, the integrated charges are transferred rapidly upward into the storage section by applying clock pulses. After all the image lines have been transferred into the storage section, another clock is applied to this section only to shift the image line by line into the readout register where they are shifted to the output stage. At the same time, the image section integrates the next field of image. When the readout of the first field is finished the second field has been transferred into the store and is ready to be readout. This cycle is repeated onward to output video signals continuously.

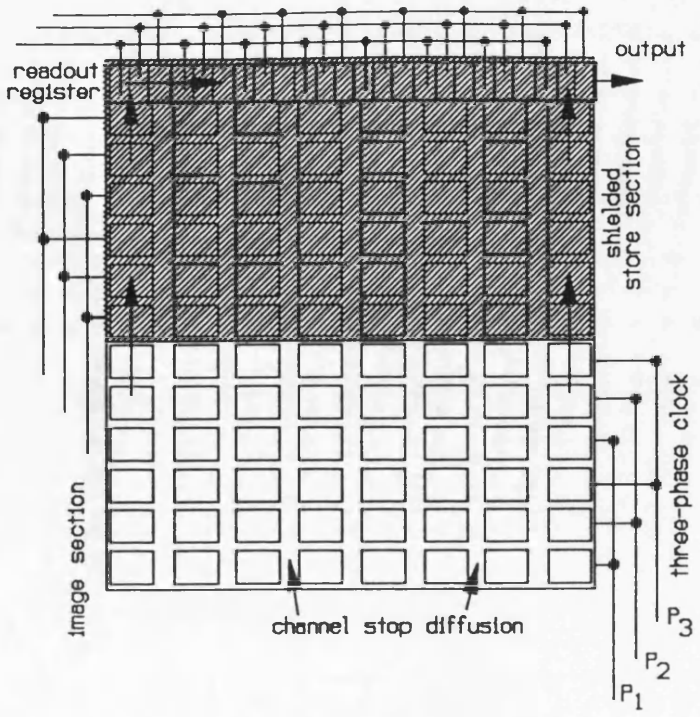

Fig.5-2 Frame transfer (FT) CCD image sensor

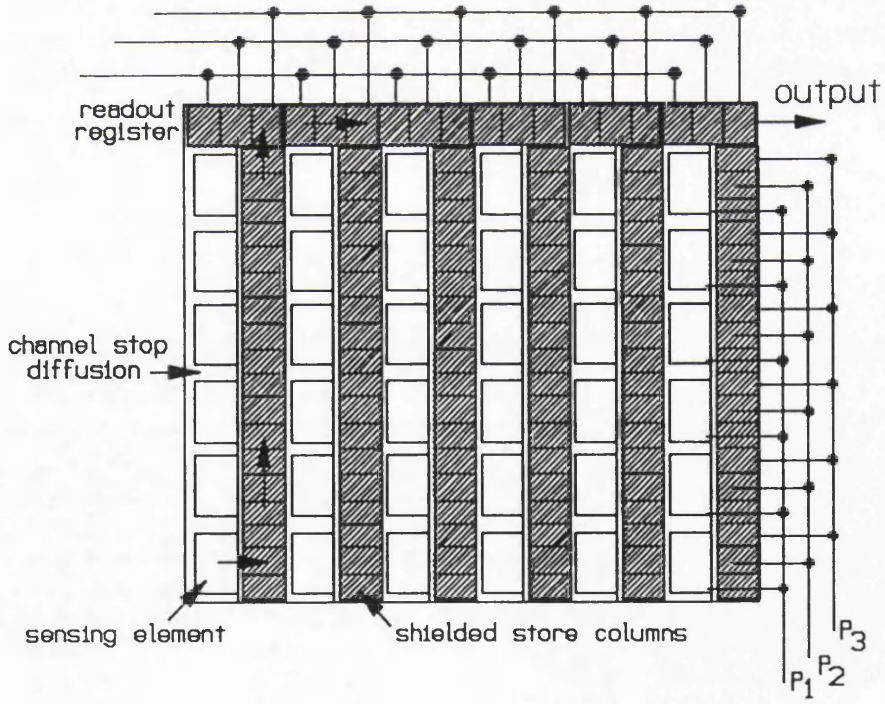

Fig.5-3 Interline transfer (ILT) CCD image sensor

In the ILT, the array is arranged so that each image column has its shielded storage column beside it. At the end of the

integration period the collected charges are all transferred horizontally to the storage columns in one step. The field of signal charge packets are then read out line by line in a manner similar to that used in the FT array. The interlace is achieved by separately releasing charges in different fields of sensing elements into the storage columns.

CCD image arrays have very good geometric accuracy, linearity, sensitivity and dynamic range. The geometric inaccuracy is found with interferometric experiment to be less than 1/100 pixel (Lenz 1989). The thermal expansion coefficient is less than 3 ppm/°K. The experiments on the linearity can be found in Curry et al (1986) and Lenz (1987). The dynamic range of modern CCD cameras can reach as high as 60 dB. Smearing is completely avoided in ILT arrays. The problem of blooming has also been well solved. Following are some properties of CCD image arrays relevant to digital photogrammetry.

Resolution. This performance is assessed in terms of the MTF (modulation transfer function),which describes the decline in image contrast with the increase of frequency of a test black and white bar pattern. The percentage of contrast at the Nyquist limit to that at zero frequency is used as a numerical measure of MTF. The MTF in horizontal direction of the ILT array is generally higher than that of the FT array due to the structural difference that the sensing region in the ILT is narrow compared with the element pitch. The ILT array has, however, a more severe aliasing effect than the FT array for the same structural reason. Aliasing is a phenomenon that a

bar pattern of a frequency higher than the Nyquist limit is reproduced in a bar pattern of lower frequency. In vertical direction, with TV interlace, the ILT array has a higher MTF than the FT array since the sensing regions used for successive fields are different in the ILT array but overlapping in the FT array. The maximum number of black and white line-pairs an FT array can virtually resolve is usually only a quarter of its quoted number of TV lines. The MTF value is dependent of the charge transfer efficiency and the extent of charge cross-talk. Long wavelength lights have deep penetration in silicon and thereby cause severe cross-talk. The red and infrared lights therefore have lower MTF than other colour lights. The resolution of a image sensor must be given more consideration when it is used to image fine detailed scene and small targets.

Non-uniformity. The element-to-element non-uniformity in signal level over the CCD array has to be considered in precision measurement applications. The non-uniformity is caused by a number of factors. Firstly, the thermally generated signal(dark signal) fluctuates over the array and contributes to the non-uniformity. Dark signal and its non-uniformity are highly temperature dependent and usually vary with time. Secondly, the complex electrode structures overlaying the CCD surface makes the sensitivity of the CCD elements (aperture response) unsmooth. This component of non-uniformity varies with the colour of incident light. Thirdly, non-uniformity arises from material variations across the CCD chip and some defective sites in the silicon chip.

5.2 Frame grabbers

The output of a CCD camera is usually analogue composite video signal of CCIR standard or RS170 standard. It is converted into digital images by the so called frame grabbers. A frame grabber is commonly made into a single board which is inserted in one of the expansion slots of the host computer when in use. It may consist of several circuits in charge of analogue image conditioning, A/D conversion, frame memory, and D/A conversion for display, as shown in Fig.5-4. The input video signal first goes through the DC restoration where its voltage drift is compensated for. The signal may be boosted or attenuated or added with a constant voltage offset by the gain and offset control circuitry. The conditioned video signal then enters the AD converter where it is sampled at constant time intervals into a series of discrete voltage values and these voltage values are classified into a given number of intensity levels (commonly 256 levels). These intensity levels are then coded and stored in the frame memory according to the addresses provided by the sampling pulses. The frame memory is accessible by the host computer directly or via a pixel buffer (for reducing the contention with display scanning). The LUT (look up table) is for pixel transformation. It is a table containing 256 values if there are, for example 256 possible intensity levels. The input pixel value is used as address and the output pixel value is the value stored at that address. The values contained in the table can be programmed according to the required transformation. With LUTs simple point transformations can be performed with no calculation or processing delay. To display the image on a video monitor, the

DAC converts the pixels into analogue video signal.

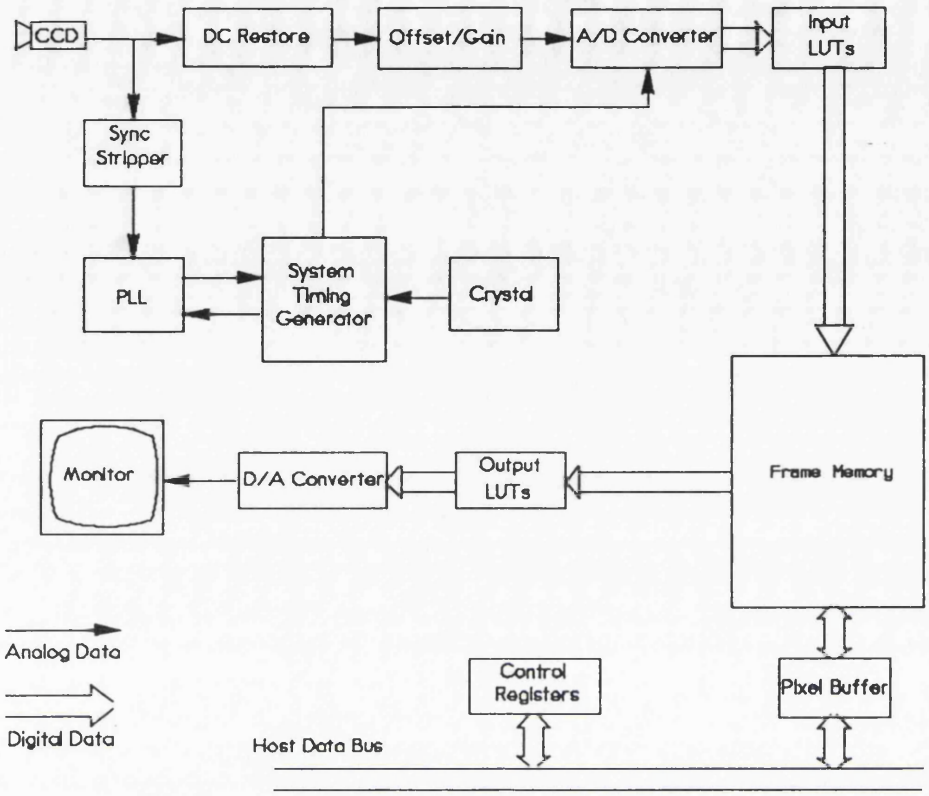

Fig.5-4 Block diagram of a frame grabber

In most systems, a phase lock loop (PLL) is used for synchronizing the video source and the frame grabber. When the composite video signal enters the frame grabber, its sync information is extracted by a sync stripper. Two successive horizontal sync signals are then detected and their time span used to derive the frequency of resampling clock, assuming a certain pixel number within an image line. A new h-sync signal is generated from the resampling clock and phase-locked to the source h-sync.

5.3 Synchronization and linejitter

The lines in digital images are actually defined by the

horizontal synchronizing signals given by the frame grabber. Any instability in the h-sync signal of the frame grabber relative to that of the camera can cause relative positional shifts in the images lines, which are called linejitter. The instability in the h-sync reference level, in terms of which the h-sync signal is detected, also contributes to linejitter. Linejitter could be as large as 1/4 pixel and vary from line to line, from image to image, being influenced by environmental factors such as temperature, electric field, magnetic field etc.. This type of error is believed to be the limiting factor for precise image metrology. In order to avoid linejitter, a common pixelclock should be used to drive both the camera and the frame grabber to generate their synchronizing signals. Unfortunately, not many CCD cameras or frame grabbers of this design are commercially available at present. CCD cameras giving digital output are also rare although this situation is changing.

For the present, a few methods have been suggested to determine and compensate for the linejitter. The method suggested by Lenz (1987) is based on the Fourier analysis of the aliasing, which emerges as a result of the interaction between the CCD clock pulses and the ADC sampling pulses. For many CCD cameras, there usually exist small but visible clock peaks on the video signal due to the imperfection of the filter. These clock peaks, aliased with the sampling pulses in the ADC, make a blank image line appear to vary periodically in intensity. The Fourier analysis on this periodical pattern for each line gives the magnitude of the linejitter as well as the ratio of the CCD cell frequency to the ADC sampling

frequency. If the clock peaks are well suppressed by the filters in some CCD cameras, a small fraction of the clock peak can be added on purpose with a bandpass filter. No accuracy was reported by the author but the linejitter values determined in his experiment were shown to be long and short term stable within 1/20 pixels.

Luhmann and Wester-Ebbinghaus (1987) used a glass plate with precise vertical lines in front of the CCD chip. This idea has been adopted in the design of some CCD cameras for photogrammetric use. Beyer (1987) used plumb vertical lines in the object space and the plumb line calibration principle.

In this project, the linejitter was presented as a worse accuracy in the sampling direction as opposed to the line direction as will be found in the later chapters. Since this lower accuracy caused by linejitter was not as bad as to hinder the pursuit of the main goal, little attempt was made to correct for it. It was considered to be better to investigate the linejitter problem in the future when a CCD with transferable pixel clock or a digital CCD is available. In fact, the problem of linejitter has already been well investigated by other researchers (Beyer,1987; Dähler,1987; and Lenz,1987,1989).

Chapter 6. Digital image processing

The tasks of digital image processing in this project involve the detection and precise location of target images, target identification and correspondence of conjugate target images. In this chapter is the description of the algorithms for those tasks, which were designed and programmed completely by the author except where mentioned otherwise.

6.1 The detection of circular target images

The target for calibration work is a black ring in white background as shown in Fig.6-1a and the target for object point is a black circle shown as Fig.6-1b. The detection of these target images is constituted by the following steps.

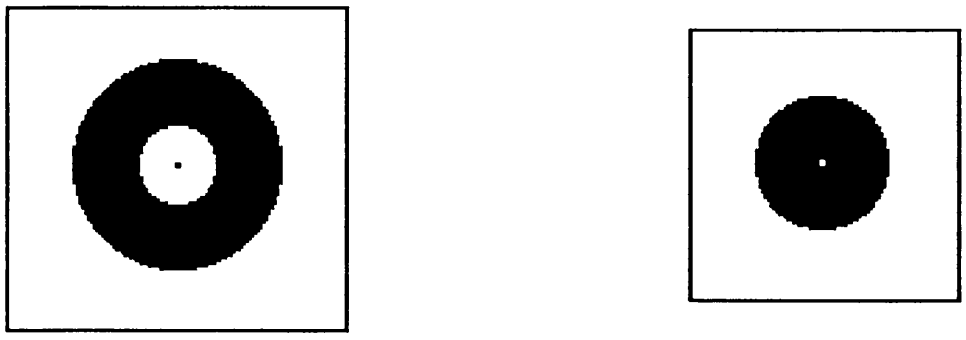

(a) (b)

Fig. 6-1. (a) Target for calibration; (b) Target for object points.

Lowpass filtering A 3×3 average filter is imposed on each frame of original image. Although it takes a large part of the total processing time, this step proved to be necessary in order to ensure a better accuracy in the later procedures

of target image location. The lowpass filtering function in the Vicar package bought with the PCVision Plus frame grabber was used, though it is very easy to program one.

Binarizing A threshold is set. All the pixels whose values are greater than this threshold are turned to 1 and all the others turned to 0. In the case of calibration using the camera-on-theodolite method, it can be arranged that the black rings of the two targets and their white background comprise a dominant part of the subimage to be processed. This simplifies the determination of threshold and naturally the mean value or the median value of the subimage is chosen as the threshold.

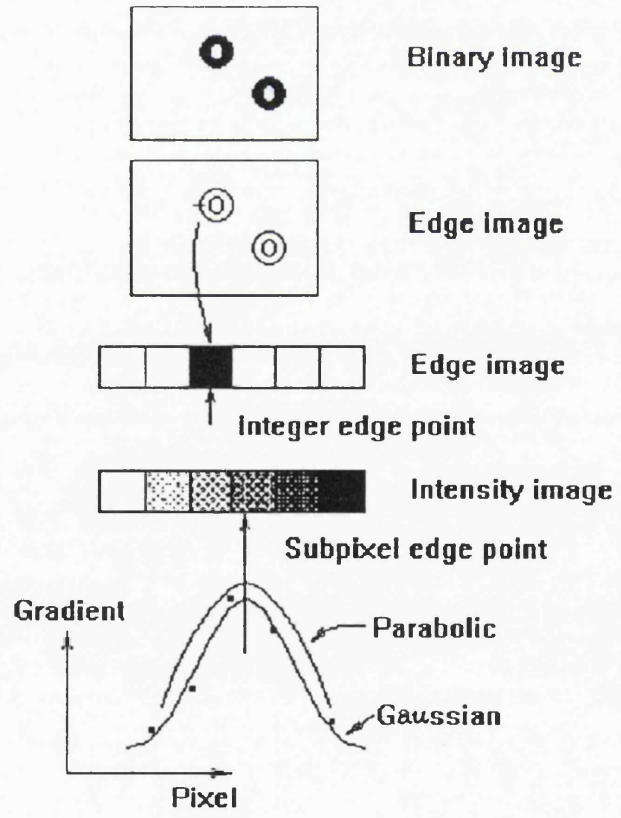

Fig. 6-2 Detection and subpixel location of target images

While determining the object points, however, the scene in which the targets are scattered is usually not evenly illuminated and shadows are often inevitable. In this case the local thresholding method is employed. In this method a small window is scanned throughout the whole image while the contrast within the window is checked against a predetermined threshold. If the contrast is greater than the threshold and the grey level of the centre pixel is lower (for detecting black target) than the median of the window this pixel is set as 1 otherwise as 0. As a part of the whole scheme, here, we chose a relatively low threshold so that all the target images are surely detected. Many false target images may thereby be involved, but they can be ruled out through the following steps.

Edge extraction Edge points are flagged with 1 and non-edge pixels with 0 using the rule that, if a black pixel has at least one white pixel among its 4-neighbours, it is an edge pixel; otherwise it is a non-edge pixel.

Edge following On the binarized edge image obtained through the above steps, scanning is carried out until an edge pixel, valued 1, is met. The coordinates of this edge pixel are recorded and its value is turned to 0. Its adjacent edge pixel is searched among its 8-neighbours (if the edge is not of one-pixel-width, the search is made anticlockwise starting from the pixel normally to the right of the preceding direction so that only the outer edge is stripped). When the adjacent edge pixel is found its coordinates are also recorded and value is set at 0. This process is continued. If it leads

back to the first edge pixel, it is indicated that a closed edge has been followed and recorded. Scanning is resumed in order to find the next edge, to which edge following will take place again. After the whole image has been scanned, all closed edges, among which are those of the targets, are stored. In practice,some constraints are imposed to rule out those edges with too long or too short perimeters so as to simplify the identification of targets.

Edge extraction can also be realised by applying standard Laplacian operator followed by zero-crossing, bridging, thinning and following.

6.2 Target image identification

Target image identification The targets for calibration are identified using the fact that their edges comprise two concentric circles. So, if two closed edges are found to have identical centroids to a given degree of accuracy, they are deemed to comprise a target. In order to identify which is the near target and which is the far target, the direction of the vector from the near target image to the far target image is input in one of the four values: north-east, south-east, south-west and north-west. The object point targets are recognized by the criterion that the root mean square residual errors of the elliptic fit of the closed edge is under a given limit and the perimeter value falls into a given band. Since the elliptic fit is not implemented until the precise location stage, a primitive identifier is used just after the detection stage which is based on the criterion that the radii to all

edge points of a target are reasonably identical.

6.3 Sub-pixel location of target images

Precise edge location The edge detection procedure described above gives the coordinates of edge points only as integers. The following interpolation algorithm is implemented to locate the edges to sub-pixel accuracy. On the filtered intensity image, for every edge pixel four to six neighbouring pixels along the normal direction at that edge pixel are used to calculate a number of gradient values. These gradient values are then fitted by a parabolic curve or a Gaussian curve using least squares. The maximum point of the fitted curve is taken as the precise sub-pixel edge point. This method is justified only under the assumption that the real continuous edge signal has its gradient symmetrical about the exact edge and this gradient function is of parabolic or Gaussian type. In fact, the assumption about symmetry is usually true because most factors causing image blur including imperfect lens, diffraction at the pupil, constant object motion, the spread of sensor sensitivity and cell cross talk, are linear and symmetrical; and the asymmetrical effect of some other factors like transfer smear on the CCD chip is small enough to be neglected. As to the type of the gradient function, either using parabola or using Gaussian function is only an approximation because the real function type is unknown. Alternatives do exist but they either take more computational time or use too many pixels which is not allowed in our case where edges are rather close to each other. In this case, the parabolic fitting and the Gaussian fitting are

both successfully used with the help of some tactics to choose the interpolating pixels and some constraints to prevent the bad estimated edge values from joining the next stage of deriving target centres.

Precise target centroid location An ellipse is fitted to each of the above determined edges by robust least square method. The centroid of the ellipse is regarded as the precise centroid of the corresponding circle. In the case of calibration, each target consists of two concentric circles so their average coordinates are obtained and taken for the final target image coordinates.

Strictly speaking, there is a deviation between the image of the target centroid and the centroid of the target image. After the author's derivation, the formula for calculating this shift is given below*.

$$\Delta = f\frac{Db^2\tan t(1+\tan^2 t)}{(D+B\tan t)^3-(D+B\tan t)b^2\tan^2 t} \qquad 6\text{-}1$$

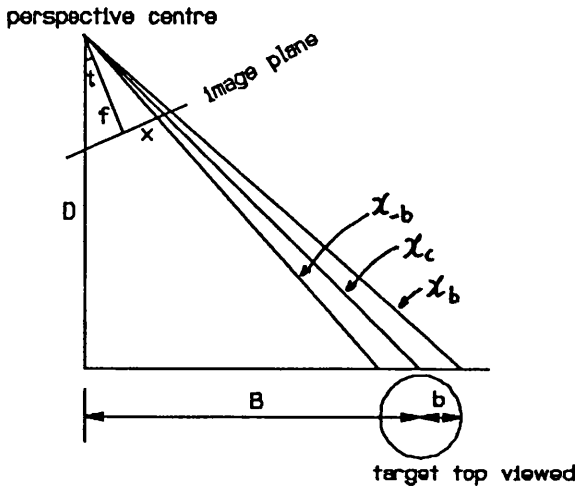

Figure 6-3. The centre of image is not the exact image of the centre

---

*From Fig.6-3 it can be seen that the image coordinate of the image of the target centre x_c can be expressed as follows,

$$x_c = f \tan(\theta - t) = f \frac{\tan\theta - \tan t}{1 + \tan\theta \tan t}$$

$$\because \tan\theta = \frac{B}{D} \quad . \qquad \therefore x_c = f \frac{B - D \tan t}{D + B \tan t} \quad .$$

Likewise the image coordinates of the images of the outer and inner edge points of the target are

$$x_b = f \frac{(B+b) - D\tan t}{D + (B+b)\tan t} \quad \textit{and}$$

$$x_{-b} = f \frac{(B-b) - D\tan t}{D + (B-b)\tan t} \quad \textit{respectively}$$

The centre of the target image detected by the computer will be the mean of the detected edge points, i.e.

$$\frac{1}{2}(x_b + x_{-b})$$

Therefore, the shift between the centre of target image and the image of target centre is

$$\Delta = x_c - \frac{1}{2}(x_b + x_{-b})$$

After substitution and rearrangement the Eq.6-1 is obtained.
It should be noted that the derived equation was only intended to be used to estimate the significance of the contribution of this type of error in the experiments.

For example, in the case of calibration,

$D = 2500, \quad B = 0, \quad b = 14, \quad f = 25, \quad \tan t = 3/25$

$\Delta = 0.095\ \mu$

$= 0.01$ pixel;

in the case of theodolite scanning photogrammetry,

$D = 3100, \quad B = 0, \quad b = 7, \quad f = 25, \quad \tan t = 2/3$

$\Delta = 0.12\ \mu$

$= 0.01$ pixel.

As is seen from the example, this deviation is too small to consider in either the case of calibration where the targets are nearly orthogonally imaged or the case of three dimensional determination where very small targets are used.

6.4 Accuracy assessment of target image location

Three measures can be used to assess the accuracy of the target image coordinates. For the calibration target, the differences between centroid coordinates of the two concentric circles comprising the target can give one measure. A large number of such differences from many images taken under various illumination conditions gave an average standard deviation for single location as 0.04 pixel in the line direction and 0.03 in the sample (see Table. 6-1). This measure mainly reflects the performance of the algorithm. The fluctuation of this measure in those different cases are due mainly to the change of illumination among those cases.

The second measure is the standard deviation of the target image coordinate obtained from many images which are taken of the same target in a stable environment. In contrast to the first measure, the second measure involves additional non-algorithm error, which is caused by the instabilities in imagery. This measure for the mean of two separate locations was found to be about 0.03 pixel in line and 0.05 in sample (see Table. 6-2).

Finally, we can use the following method, which may be called the sub-pixel shift method, to acquire the third measure of the accuracy of target image location. The target and the camera are set up in a stable environment. While repeatedly translating the target or the camera by such a amount that the target image shifts by a constant sub-pixel increment along the coordinate direction being tested, a

number of images of the target are recorded. Target location is then implemented for all the images to determine their centroid coordinates. Without error, the coordinates of the target images from two successive frame of images should differ, in the direction under test, by the applied increment. Thus, a standard deviation is obtained from a linear regression with all those data. This measure reflects the performance of the target location algorithm in different spatial phase of a pixel as well as the instability in imagery. It can be regarded as the last comprehensive measure to assess the target image coordinates before entering calibration stage. In our work the camera was translated by rotating its carrier theodolite, in which an approximation is tolerable. The increment was chosen to be 0.1 pixel and the resulting standard deviations were around 0.03 pixel in line and 0.06 in sample for the calibration targets. Table 6-3 shows a sample of the test results.

Table 6-1. **Standard Errors of Target Image Coordinates**
(for outer or inner circle location, unit: pixel)

Case	X		Y		Number of images
	Target 1	Target 2	Target 1	Target 2	
2191100	0.051	0.043	0.017	0.019	7
2191200	0.051	0.050	0.012	0.017	14
2191226	0.035	0.045	0.038	0.026	16
2201109	0.025	0.029	0.023	0.018	18
2201030	0.028	0.038	0.012	0.023	9
2121220	0.020	0.029	0.018	0.012	15
2201130	0.035	0.051	0.014	0.014	9
2201150	0.051	0.074	0.069	0.016	13
2201220	0.026	0.036	0.059	0.019	10
2201248	0.064	0.049	0.013	0.032	10
2201620	0.027	0.032	0.044	0.029	86
mean	0.040	0.042	0.031	0.020	
Mean	0.041		0.026		

Table 6-2. **Standard Errors from Residuals of Different Images**
(reflecting the variation among images, unit: pixel)

Case	X		Y		Number of images
	Target 1	Target 2	Target 1	Target 2	
2191100	0.013	0.025	0.026	0.017	7
2191200	0.019	0.022	0.034	0.047	14
2191226	0.048	0.039	0.071	0.066	16
2201109	0.026	0.021	0.058	0.059	18
2201030	0.032	0.024	0.041	0.064	9
2201130	0.028	0.025	0.046	0.032	9
2201220	0.033	0.036	0.021	0.021	10
2201248	0.044	0.020	0.044	0.035	10
2201620	0.029	0.024	0.067	0.060	86
mean	0.030	0.026	0.045	0.045	
Mean	0.028		0.045		

Table 6-3. **Standard Errors from Residuals of Linear Regression in the Sub-Pixel Shift Method**

(only a sample of the results, unit: pixel)

Cases	X		Y		Number of residuals
	Target 1	Target 2	Target 1	Target 2	
1	0.027	0.019	0.044	0.037	11
2	0.029	0.033	0.072	0.069	21
3	0.048	0.049	0.061	0.042	11
4	0.021	0.016	0.048	0.076	11
5			0.067	0.075	20
mean	0.031	0.029	0.058	0.060	
Mean	0.030		0.059		

6.5 Correspondence of conjugate target images

Once we have located all the target images on a pair of stereo images, we need to determine which target image on the right image comes from the same object target as a given target image on the left image. Given the coordinates of a target image on the left image, we can determine its epipolar line on the right image using the interior and relative orientation parameters of the two images. In our case, those parameters are known with a high accuracy, hence the target image nearest to the epipolar line is considered to be the conjugate target image.

Suppose that the principal distances, the rotation matrices and the translation vectors for the left and right images are f_l, $\boldsymbol{R}_l$, $\boldsymbol{T}_l$ and f_r, $\boldsymbol{R}_r$, $\boldsymbol{T}_r$ respectively as defined in

Eq.2-8 with the original subscripts removed. The epipolar line on the right image for a given point (x_l', y_l') on the left image is derived as the following expression:

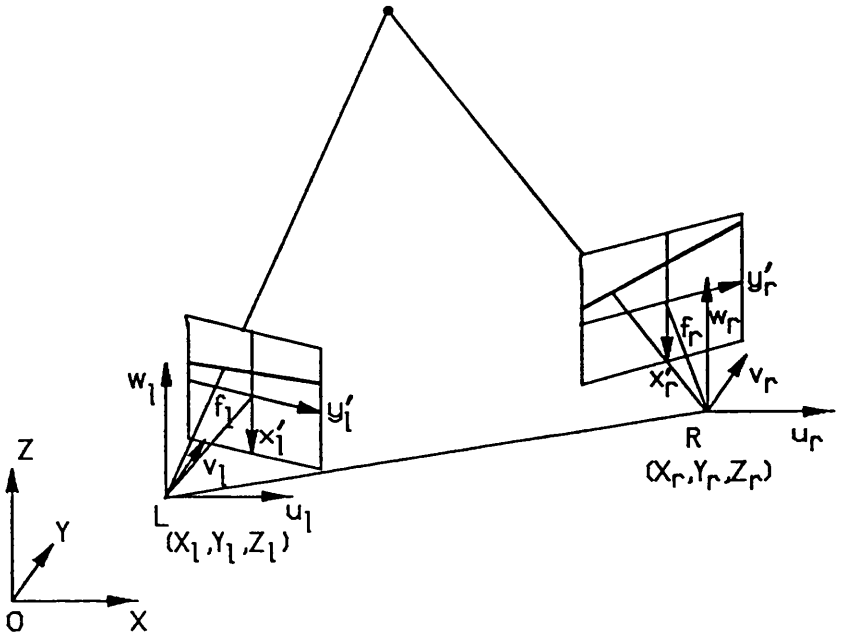

Figure 6-4. Epipolar lines

$$E\,x_r' + F\,y_r' - G\,f_r = 0 \qquad 6\text{-}2$$

$$\begin{pmatrix} E \\ F \\ G \end{pmatrix} = \boldsymbol{R}_r^T \begin{pmatrix} B_y w_l - B_z v_l \\ B_z u_l - B_x w_l \\ B_x v_l - B_y u_l \end{pmatrix}, \qquad \begin{pmatrix} u_l \\ v_l \\ w_l \end{pmatrix} = \boldsymbol{R}_l \begin{pmatrix} x_l' \\ y_l' \\ -f_l \end{pmatrix}, \qquad \boldsymbol{B} = \begin{pmatrix} B_x \\ B_y \\ B_z \end{pmatrix} = \boldsymbol{T}_r - \boldsymbol{T}_l$$

It is quite possible that there will appear more than one point all very close to the epipolar line and also that the closest point is not necessarily the conjugate point. Other criteria are therefore required to resolve this problem. In our experimentation the criterion that no intersected object point should exceed a predetermined depth of field is used, which may not apply to other cases. A more common method is

using the correlation technique in which the correlation functions at those points which are close to the epipolar line are compared and the point with the strongest correlation is taken for the conjugate point. If the intensity correlation is used the window should be so large as to include sufficient surrounding texture for a reliable match since the man made targets are of the same pattern and a convergent imaging configuration is usually adopted. The most difficult case is when the targets are hung in space and without any supporting texture.

Chapter 7. Experiments in theodolite scanning photogrammetry

7.1 Objectives and method of experiments

The objective of the experiments was to test the accuracy of the experimental theodolite-CCD camera system in three dimensional measurement using the theodolite scanning principle. The experiments were to involve all the techniques developed and discussed in the previous chapters. It was expected that an accuracy improvement would be achieved over the non-scanning cases with only a pair of images when measuring an object of a specified size. This accuracy improvement, if achieved, would also serve as evidence of the feasibility of theodolite scanning photogrammetry and the success of the methods and algorithms proposed in the other chapters.

The measured object in the experiments was a three dimensional target array spread over a volume of 2.3×1.7×0.9 m. For the purpose of accuracy assessment, the coordinates of all the targets were also determined with Kern E2 - ECDS system to an accuracy of 0.01 mm in X and Z and 0.05 mm in Y, the depth, and these coordinates were treated as true values. The accuracy of the photogrammetrically determined coordinates was assessed by the RMS of residuals resulting from the similarity coordinate transformation from the true coordinates to the determined coordinates.

Two theodolite stations were set up at a stand-off distance of 3 metres and a base length of 2 metres. The

Philips frame transfer CCD camera was used. The dimensions of the CCD chip was 4.5×6.0 mm and the number of sensing elements of the chip was 588×604. A PCVISION Plus image grabber was used to give digital images of 480×512 pixels and 256 grey levels for each pixel. The dimensions of a pixel were approximately 8.1 microns in x and 11.6 microns in y. Only one camera was available; hence it had to be mounted on the two theodolites in turn and the environment had to be kept highly stable. The lens of 25 mm focal length was used. The gain and offset control of the image grabber was switched on.

The scanning photogrammetry started with the theodolite orientation using one of the methods introduced in chapter 4. The camera was then mounted on the left theodolite followed by the camera calibration using the camera-on-theodolite method. The target to theodolite distances for the calibration were obtained through theodolite triangulation which could be integrated in the orientation stage. The scanning image capture was carried out immediately after the calibration. The same procedures were then repeated for the right station. For each station 3 × 3 frames of image were taken to cover the whole area to be measured (see Fig.2-2).

7.2 Details of experiments and results

In the following, the procedures of a whole set of experiment - the Experiment 1 - are described step by step with input and output data shown for each step.

1) Check for warm-up effect, environmental stability and instrument errors. The warm-up effect and environmental stability were checked in the same way as assessing the accuracy of target image location described in Chapter 6. No environmental instability was found. The warm-up effect diminished to an insignificant level twenty minutes after the camera was switched on. The theodolites were tested and adjusted for collimation error and transit axial inclination; and the dual axial compensators were switched on. All angles were observed with face-left only. The unit of angles is gon..

2) Theodolite orientation:

Definition of the object coordinate system O_w-$X_wY_wZ_w$: Origin O_w is the rotational centre of the left theodolite. X_w axis is horizontal and pointing at the vertical axis of the right theodolite as positive. Z_w axis is the vertical line through O_w and pointing upwards.

The method of horizontal reciprocal pointing and pointing at one object point, described in Chapter 4, was used to determine the rotation matrices and the translation vectors between the object coordinate system and the theodolite coordinate systems, ie. R_t and T_t for both the theodolites. The horizontal reciprocal pointing was achieved by sighting the pins erected on top of each other's theodolites and as near to the vertical axes as possible. Each pin was sighted twice. After the first sighting the target theodolite was turned by 180° before the second sighting. The two readings thus taken were then meaned as the direction of the centre of the target

theodolite. The horizontal distance between the two theodolites was obtained from previous data. Its accuracy was not critical because the scaling accuracy was not to be assessed in the experiments. The observation values and results are shown in Table 7-1 and Table 7-2 respectively.

Table 7-1 **Observations of theodolite orientation**

	LHS theod.		RHS theod.	
Sighted target:	H(gon)	V(gon)	H(gon)	V(gon)
R.theod.	199.9332			
L.theod.			399.1647	
Obj.point	119.1459	296.5190	81.2224	296.8756
L.theod-R.theod horizontal distance: 2289.770 mm				
Extra observations for determining target theodolite distances for subsequent system calibration:				
L.near target	95.9222	294.3288	53.2305	296.1300
L.far target	94.6796	294.4830	62.0715	295.6884
R.near target	155.2043	297.4872	109.0955	296.8223
R.far target	139.4830	296.4606	107.8056	296.0642

Table 7-2 **Result of theodolite orientation**

R_t^T (Left theodolite)

1.049345325615993E-003	9.999994494370422E-001	0.000000000000000E+000
-9.999994494370422E-001	1.049345325615993E-003	0.000000000000000E+000
0.000000000000000E+000	0.000000000000000E+000	1.000000000000000

T_t (left theodolite)

0.000000000000000E+000	0.000000000000000E+000	0.000000000000000E+000

R_t^T (Right theodolite)

1.312053860761503E-002	9.999139220286145E-001	0.000000000000000E+000
-9.999139220286145E-001	1.312053860761503E-002	0.000000000000000E+000
0.000000000000000E+000	0.000000000000000E+000	1.000000000000000

T_t (right theodolite)

2289.770000000000000	0.000000000000000E+000	-23.589295037449980

3) Calibration of the LHS theodolite-CCD camera

The CCD camera was mounted on the LHS theodolite. The camera-on-theodolite calibration was then carried out. Two targets were used and 16 (4×4) target images were created from each target by means of theodolite rotation. The observation values and calibration results are shown below. All the v values are vertical angles instead of raw readings. h_0, v_0 are the mean values of three repetitive observations. Note that the image x and y coordinates shown in Table 7-3 were then shifted by 240 and 256 respectively and x scaled by 0.7 before entering the calibration program (for the detail see Appendix: Camera Calibration Certificate)

Table 7-3 **Input data of calibration on the LHS**

```
17
32                                          -- total number of image points.
95.92130   -5.67111   94.67880   -5.51700 -- h0.near, v0.near, h0.far, v0.far.

2820.460                 -- target-theod. distance for odd-number points.
4002.063                 -- target-theod. distance for even-number points.

  1 i     59.11642   443.93090  -- detected image coordinates x y in pixel
  1 r     91.60940   -10.30540  -- theodolite readings h v in gon.
  2 i     33.58029   399.99680
  2 r     91.60940   -10.30540
```

3 i	175.91700	443.36080	18 i	30.87593	144.64860
3 r	91.60940	-8.04150	18 r	99.00060	-10.34180
4 i	149.72020	399.48900	19 i	177.02010	186.99800
4 r	91.60940	-8.04150	19 r	99.00070	-7.98810
5 i	297.48510	442.95640	20 i	151.62710	144.74680
5 r	91.60950	-5.68210	20 r	99.00070	-7.98810
6 i	270.59710	399.08460	21 i	296.17670	186.75660
6 r	91.60950	-5.68210	21 r	99.00070	-5.67580
7 i	.41030	442.85250	22 i	270.05090	144.56140
7 r	91.60950	-3.35490	22 r	99.00070	-5.67580
8 i	389.76550	398.91280	23 i	420.80300	186.46530
8 r	91.60950	-3.35490	23 r	99.00070	-3.25850
9 i	59.94474	313.89600	24 i	393.87380	144.23790
9 r	95.35090	-10.25990	24 r	99.00070	-3.25850
10 i	34.87020	270.87640	25 i	55.91154	62.12443
10 r	95.35090	-10.25990	25 r	102.58770	-10.35560
11 i	177.32240	313.62360	26 i	31.59383	20.09070
11 r	95.35090	-7.98620	26 r	102.58770	-10.35560
12 i	151.56210	270.71260	27 i	176.77600	62.11069
12 r	95.35090	-7.98620	27 r	102.58780	-8.01220
13 i	297.03630	313.38700	28 i	151.67500	20.24312
13 r	95.35090	-5.66380	28 r	102.58780	-8.01220
14 i	270.54650	270.46320	29 i	299.11540	61.98560
14 r	95.35090	-5.66380	29 r	102.58770	-5.63620
15 i	417.85210	313.14860	30 i	273.27190	20.27446
15 r	95.35100	-3.32030	30 r	102.58770	-5.63620
16 i	390.59760	270.26410	31 i	417.50610	61.67512
16 r	95.35100	-3.32030	31 r	102.58770	-3.33780
17 i	55.53445	187.05750	32 i	390.83450	19.96152
17 r	99.00060	-10.34180	32 r	102.58770	-3.33780

Table 7-4 **Result of calibration on the LHS**

Translations T_o in mm:	-.433	60.657	52.773
Rotations ϕ,ω,κ in radian *:	-.48916697E+01	.15646143E+01	.33240654E+01
Rotation matrix R_o^T:			
	.00318859	-.00112180	-.99999429
	.99997642	-.00607938	.00319535
	-.00608293	-.99998089	.00110239
Principal distance f in pixel:	2247.899		
Principal point x_0,y_0 in pixel **:	-.8450	50.5294	
AP(1-3) radial distortion k_1,k_2,k_3 **:	.269E-12 (10^5pixel^{-2})	0	0
AP(4-5) tangential dist. p_1,p_2 **:	0	0	
AP(8-9) affine deform. A, B (10^2) **:	-.154E-07	.377E-03	

σ_0 = .0542655 RMSX= .0215717 RMSY= .0657257 (pixels)

* Rotation angles in the ϕ-ω-κ rotation system which is different from the one defined and used in other chapters. Note that it is the rotation matrices that are used in data transmission and calculation.
** Refer to Eq.3-6 and the Appendix for the use of these parameters. Note that the raw image coordinates in pixels must be shifted 240 in x and 256 in y and scaled by 0.7 in x before using these calibration values.
σ_0 -- Estimated standard deviation of unit weight with x and y being equally weighted.

4) Image capture on the LHS station

Immediately after calibration, nine (3×3) images were captured while the theodolite was "scanned" manually to the following positions respectively:

Table 7-5. **Theodolite readings for the 3×3 images on the LHS**

L1.h=111.3566(gon) v=307.0213(gon)*	L2. h=122.7744 v=302.9222	L3. h=135.7504 v=305.7253
L4. h=111.3565 v=297.1603	L5. h=122.7744 v=295.3427	L6. h=135.0170 v=296.7092
L7. h=110.0506 v=287.6379	L8. h=122.8966 v=287.5332	L9. h=135.0169 v=288.9442

* The vertical angles are obtained by subtracting 300 gons from the v values shown in the table.

5) Calibration of the RHS theodolite-CCD camera

The CCD camera was detached from the LHS theodolite and mounted on the RHS theodolite. The same calibration procedures as the step 3 were then carried out with the RHS theodolite-CCD camera. The observations and results are shown as follows:

Table 7-6. **Input data of calibration on the RHS**

```
17
32                                          -- total number of image points.
109.09520  -3.17801  107.80560  -3.93579  -- h0.near, v0.near, h0.far, v0.far.

2667.018                    -- target-theod. distance for odd-number points.
3997.513                    -- target-theod. distance for even-number points.

  1 i     57.24527    444.69550  -- detected image coordinates x y in pixel
  1 r    104.75310     -7.93740  -- theodolite readings h v in gon.
  2 i     75.25411    398.58170
  2 r    104.75310     -7.93740
```

3 i	181.86320	443.96650	18 i	76.47541	141.71620
3 r	104.75310	-5.52470	18 r	112.18270	-7.87770
4 i	198.92670	397.97660	19 i	182.13980	185.46030
4 r	104.75310	-5.52470	19 r	112.18270	-5.47140
5 i	302.11290	443.57160	20 i	199.82890	141.49280
5 r	104.75310	-3.19360	20 r	112.18270	-5.47140
6 i	318.31120	397.51690	21 i	301.57860	185.17570
6 r	104.75310	-3.19360	21 r	112.18280	-3.15600
7 i	429.80350	443.03490	22 i	318.36820	141.19070
7 r	104.75310	-.71940	22 r	112.18280	-3.15600
8 i	445.09320	397.19520	23 i	430.71700	184.55360
8 r	104.75310	-.71940	23 r	112.18280	-.65430
9 i	58.63536	314.05110	24 i	446.57290	140.58880
9 r	108.50370	-7.87650	24 r	112.18280	-.65430
10 i	76.96037	269.12090	25 i	58.93625	60.91515
10 r	108.50370	-7.87650	25 r	115.74470	-7.85720
11 i	181.90390	313.66950	26 i	78.01138	18.02845
11 r	108.50370	-5.49150	26 r	115.74470	-7.85720
12 i	199.25790	268.81020	27 i	181.44330	61.05629
12 r	108.50370	-5.49150	27 r	115.74480	-5.48520
13 i	298.79210	313.20430	28 i	199.49990	17.92061
13 r	108.50370	-3.22640	28 r	115.74480	-5.48520
14 i	315.29920	268.29860	29 i	300.72420	60.76646
14 r	108.50370	-3.22640	29 r	115.74480	-3.17150
15 i	424.17140	312.45300	30 i	317.82320	17.43875
15 r	108.50370	-.79750	30 r	115.74480	-3.17150
16 i	439.82060	267.78830	31 i	428.03490	60.00859
16 r	108.50370	-.79750	31 r	115.74480	-.70250
17 i	57.77563	185.61270	32 i	444.23670	16.57516
17 r	112.18270	-7.87770	32 r	115.74480	-.70250

Table 7-7 Result of calibration on the RHS

Translations T_o in mm: -.433 58.788 52.803

Rotations ϕ,ω,κ in radian *: -.41293951E+01 .15655098E+01 .25640781E+01

Rotation matrix R_o^T:

.00548572	.00288612	-.99998079
.99997521	-.00442914	.00547291
-.00441326	-.99998603	-.00291035

Principal distance f in pixel: 2248.619

Principal point x_0,y_0 in pixel **: -9.2269 45.9483

AP(1-3) radial distortion k_1,k_2,k_3 **: .200E-12 (10^5pixel^{-2}) 0 0

AP(4-5) tangential dist. p_1,p_2 **: 0 0

AP(8-9) affine deform. A, B (10^2) **: -.167E-05 .380E-03

σ_0 = .0786117 RMSX= .0280477 RMSY= .0962056 (pixels)

* Rotation angles in the ϕ-ω-κ rotation system which is different from the one defined and used in other chapters. Note that It is the rotation matrices that are used in data transmission and calculation.
** Refer to Eq.3-6 and the Appendix for the use of these parameters. Note that the raw image coordinates in pixels must be shifted 240 in x and 256 in y and scaled by 0.7 in x before using these calibration values.
σ_0 -- Estimated standard deviation of unit weight with x and y being equally weighted.

6) Image capture on the RHS station

Immediately after calibration, nine (3×3) images were captured while the theodolite was "scanned" manually to the following positions respectively:

Table 7-8 **Theodolite readings for the 3×3 images on the RHS**

R1. h=69.5183(gon) v=306.2077(gon)*	R2. h=82.2921 v=303.5064	R3. h=93.2775 v=307.9348
R4. h=70.1825 v=298.0181	R5. h=81.5576 v=295.5792	R6. h=93.2773 v=297.6759
R7. h=70.5567 v=288.9606	R8. h=81.5574 v=288.1198	R9. h=93.5201 v=287.8257

* The vertical angles are obtained by subtracting 300 gons from the v values shown in the table.

7) Automatic target image location by the computer. The computer program for target image location was executed for each of all the captured images from both stations. The image coordinates of all the located target images are listed below. They must be shifted and scaled the same way as in the calibration before they can be used directly with the calibrated valued obtained in step 3 and 5. The unit is sampling pixel.

Table 7-9 **Target image coordinates located by the computer**

LHS station				RHS station			
	x	y	image number		x	y	image number
6			1	4			1
1	40.550	99.609		1	61.842	77.530	
2	209.242	50.314		2	192.132	476.035	
3	228.361	266.162		3	194.586	295.291	
4	403.360	193.184		4	360.607	413.283	
5	384.263	439.108		13			2
6	414.279	437.983		1	49.063	37.339	
12			2	2	219.015	135.747	
1	39.511	151.570		3	10.476	466.350	
2	201.651	43.709		4	50.471	300.609	

3	58.536	389.367		5	189.056	263.350	
4	211.725	505.808		6	221.631	416.127	
5	218.036	319.915		7	372.968	132.342	
6	360.565	40.578		8	437.763	58.987	
7	361.322	227.112		9	467.616	129.894	
8	429.261	149.924		10	372.758	316.513	
9	458.365	38.619		11	374.186	412.630	
10	363.163	316.878		12	401.939	298.698	
11	429.116	399.634		13	442.899	299.310	
12	178.396	174.965		9			3
4			3	1	232.519	181.155	
1	176.475	166.411		2	68.615	394.329	
2	197.088	150.398		3	223.338	451.644	
3	71.073	364.472		4	271.408	180.271	
4	352.650	57.778		5	359.685	97.047	
10			4	6	412.619	35.569	
1	45.366	97.447		7	444.084	35.292	
2	86.877	14.580		8	249.126	431.426	
3	131.401	49.846		9	431.374	317.038	
4	67.378	436.999		4			4
5	81.753	487.131		1	75.717	52.152	
6	133.983	293.154		2	155.577	273.891	
7	317.525	189.181		3	160.490	479.510	
8	275.797	432.352		4	328.716	386.949	
9	310.627	432.694		9			5
10	443.566	389.953		1	32.344	85.779	
8			5	2	169.712	154.017	
1	41.250	150.396		3	36.946	326.286	
2	181.907	37.052		4	190.668	434.290	
3	218.864	169.371		5	213.947	282.014	
4	41.367	400.516		6	216.049	337.559	
5	186.956	313.933		7	333.627	173.682	
6	217.638	508.076		8	401.926	107.132	
7	419.963	133.357		9	416.250	306.565	
8	396.452	404.897		8			6
6			6	1	25.291	33.329	
1	111.077	190.882		2	72.097	32.548	
2	33.687	389.286		3	144.585	192.023	
3	285.460	85.678		4	52.563	393.359	
4	427.610	190.309		5	150.254	455.049	
5	450.533	204.749		6	295.543	28.329	
6	456.840	390.031		7	442.472	46.429	
11			7	8	341.208	320.523	
1	11.140	143.190		8			7
2	20.025	44.579		1	23.248	220.044	
3	64.437	146.247		2	43.997	41.314	
4	213.925	219.238		3	66.571	486.762	
5	32.927	362.407		4	218.615	359.322	
6	206.172	469.497		5	293.683	157.223	
7	405.551	65.337		6	422.937	242.884	
8	463.432	80.062		7	340.105	456.168	
9	323.865	264.357		8	448.664	452.384	
10	328.752	289.446		10			8
11	438.261	328.862		1	20.154	107.820	
10			8	2	198.539	209.677	
1	20.104	129.682		3	34.291	307.979	
2	201.272	31.389		4	216.121	454.196	
3	155.663	507.829		5	295.098	81.449	
4	176.264	271.957		6	361.520	81.290	
5	383.125	143.941		7	404.053	81.742	
6	411.662	147.360		8	314.412	340.262	
7	265.477	446.060		9	322.067	366.507	
8	267.601	469.005		10	430.746	320.271	
9	340.414	385.101		11			9
10	380.949	392.916		1	23.742	190.886	
8			9	2	199.927	46.040	
1	30.464	191.164		3	35.961	463.400	
2	53.459	205.443		4	57.331	386.064	
3	225.468	93.692		5	210.203	318.959	
4	58.787	390.927		6	318.955	262.156	
5	339.792	55.914		7	436.827	184.555	
6	379.411	190.120		8	318.943	262.421	
7	429.673	185.620		9	324.718	291.171	
8	296.309	318.148		10	404.238	437.487	
				11	459.764	430.487	

* -- The units of x and y are the raw line number and sample number respectively.

8) Computation of exterior orientation parameters for each image with respect to the local object coordinate system. This was the computation of R_{cw} and T_{cw} using Eq.2-9 and Eq.2-10 where R_t and T_t had already been determined in step 2, R_c and T_c in step 3 and 5, and R was computed by using Eq.2-5 with theodolite readings h and v which had been recorded in step 4 and 6.

9) Correspondence and space intersection Using the image coordinates and orientation parameters obtained in the precedent steps, the computer matched the conjugate image points and then carried out space intersection to compute the three dimensional coordinates of the object points. For each image point on each image captured on the LHS station, all images captured on the RHS station were searched for the corresponding points. Because of the small overlapping areas between adjacent "scanned" images on each station, there were more than one points matched and more than one three dimensional determinations for those points that fell into the overlapping areas. For each of those points, only one set of three dimensional coordinates was arbitrarily chosen to joint the accuracy assessment.

Although the correspondence between conjugate image points was completed automatically, the correspondence between the points and their names were accomplished manually by viewing and cross-referencing the image and the scene. The result is as follows where the unidentified matched points have been removed.

Table 7-10 **Points matched and their object coordinates**

File name: OBJCDCRP.DAT Unit: mm

Point name	Matched image point number	X	Y	Z
L1 R1 4*				
POINT K2H	1 1	286.173	3163.336	594.512
POINT C3H	2 3	274.714	4021.506	527.612
POINT C3AH	3 2	676.795	4018.330	512.702
POINT CD3	4 4	541.214	4018.645	290.317
L2 R2 9				
POINT C4H	1 4	1214.506	4014.943	497.114
POINT X11H	2 2	955.175	3815.431	271.216
POINT X14H	5 6	1482.038	3812.371	262.410
POINT X21H	6 7	950.780	3814.496	80.334
POINT X23H	7 10	1300.303	3812.520	81.404
POINT D5H	8 13	1214.584	4015.373	-5.331
POINT X31	9 9	947.650	3813.013	-36.654
POINT X24H	10 11	1476.281	3811.808	80.004
POINT X12H	12 5	1199.472	3813.825	305.226
L3 R3 4				
POINT C5	1 3	2211.639	4007.335	547.788
POINT C5H	2 8	2174.388	4008.348	516.188
POINT L2H	3 2	2144.177	3168.180	593.476
POINT CD6	4 9	1964.216	4010.258	290.509
L4 R4 4				
POINT K3H	1 1	287.856	3162.855	93.991
POINT D3H	3 2	277.733	4021.638	.233
POINT D4H	6 3	728.132	4021.080	-2.690
POINT DE3	7 4	533.450	4018.033	-231.013
L5 R5 5				
POINT D5H	1 3	1214.518	4016.036	-5.366
POINT X41H	2 2	942.823	3811.902	-170.368
POINT X42H	3 5	1188.192	3810.395	-219.717
POINT X44H	5 4	1468.837	3809.608	-185.475
POINT E4H	7 9	1179.266	4014.610	-492.588
L6 R6 3				
POINT D7H	1 5	2214.100	4011.972	-9.922
POINT L3H	2 4	2140.018	3166.937	91.702
POINT DE6	3 8	1969.922	4010.795	-247.501
L7 R7 7				
POINT E3H	2 1	182.578	4019.610	-463.575
POINT K4H	3 2	290.711	3161.742	-400.479
POINT EF3	4 4	502.930	4016.005	-714.707
POINT E3AH	5 3	773.192	4016.747	-489.871
POINT F1H	8 6	238.140	4016.769	-1029.737
POINT J3H	10 5	503.705	3180.468	-675.325
POINT F2H	11 8	712.328	4013.543	-1013.987
L8 R8 6				
POINT E4H	1 3	1179.246	4014.474	-492.635
POINT EF4	2 2	982.489	4013.831	-717.218
POINT EF5	4 4	1467.622	4012.139	-713.653
POINT F3H	6 10	1208.314	4012.113	-1013.765
POINT J5	7 8	1462.744	3180.073	-671.497
POINT J5H	8 9	1503.829	3180.252	-676.856
L9 R9 6				
POINT E5H	2 3	2245.461	4008.358	-490.800
POINT EF6	3 5	1982.256	4010.000	-715.277
POINT L4H	4 4	2142.727	3163.952	-404.933
POINT F5	6 10	2206.492	4009.133	-958.952
POINT F5H	7 11	2194.736	4008.533	-1031.475
POINT J6H	8 9	2005.289	3180.913	-678.309
L2 R3 1				
POINT C4BH	3 4	1708.264	4013.514	491.354
L5 R6 3				
POINT D6H	4 3	1730.998	4013.891	-6.132
POINT X44H	5 6	1469.050	3810.160	-185.513
POINT DE6	6 8	1969.834	4011.912	-247.520
L5 R9 1				
POINT E4BH	8 1	1743.069	4011.560	-484.599

* -- For image L1 and image R1, 4 points have been matched.

10) Accuracy assessment The accuracy of the three dimensional coordinates determined as shown above was assessed with the "true" coordinates determined using the ECDS system. The true coordinates are listed below followed by the residuals resulting from three dimensional similarity transformation from the true coordinates to the determined coordinates. The similarity transformation was implemented on the existing software on the ECDS system.

Table 7-11 **Object coordinates determined by the ECDS (mm)**

Name	X	Y	Z
C3	268.9777	3992.4992	555.4727
C5	2266.0106	3979.3603	549.6818
C3H	328.7305	4018.9425	529.2279
C3AH	730.9468	4009.7291	514.1024
C4H	1268.8991	3999.7148	498.5040
C4BH	1762.8231	3991.4927	492.6995
C5H	2228.8656	3980.9238	517.6722
CD3	595.2418	4012.0496	291.5864
CD6	2018.7728	3985.3285	291.8221
D3H	331.5256	4018.2028	1.5995
D4H	781.8557	4011.2447	-1.4053
D5H	1268.7977	4000.3391	-4.1297
D6H	1785.4053	3991.5527	-4.9110
D7H	2268.6944	3982.8942	-8.6561
DE3	587.4639	4011.4462	-229.8336
DE6	2024.2980	3985.5132	-246.2662
E3H	236.8413	4017.9213	-462.5070
E3AH	827.2446	4006.1799	-488.8796
E4H	1233.4456	3999.3427	-491.6019
E4BH	1797.5527	3989.4886	-483.6004
E5H	2299.9103	3978.8579	-489.7983
EF3	557.2535	4010.0236	-713.8347
EF4	1036.3966	4001.2773	-716.1731
EF5	1521.8074	3993.8469	-712.7389
EF6	2036.4047	3983.1418	-714.2733
F1H	292.0377	4013.1029	-1028.5171
F2H	766.2646	4003.8099	-1013.0081
F3H	1262.5381	3997.2007	-1013.1431
F4H	1783.8820	3987.2932	-1014.3495
F5H	2249.2088	3979.7308	-1030.6143
J6	2005.6744	3155.7570	-672.9281
J3H	546.3861	3173.6966	-674.5940
J4H	1085.3927	3166.7090	-676.8515
J5H	1546.7875	3160.8789	-676.2041
K2H	328.7983	3159.7489	595.8644
K3H	330.2504	3159.3393	95.0646
K4H	333.0326	3157.9435	-399.4497
L2H	2187.1093	3139.9149	594.8359
L3H	2183.2913	3139.1942	92.8088
L4H	2185.7422	3136.0199	-404.0907
X11H	1006.4319	3803.0077	272.5586
X12H	1250.8953	3798.3486	306.4861
X14H	1533.3265	3792.4310	263.6985
X21H	1002.0472	3801.5761	81.5211
X23H	1351.5969	3795.1727	82.5404
X24H	1527.5219	3791.7473	81.2615
X41	995.3652	3799.6373	-211.0905
X41H	994.4556	3799.9622	-169.2193
X42H	1239.6314	3795.3468	-218.5679
X44H	1520.6183	3790.3850	-184.4613

Table 7-12 Accuracy of the determined object coordinates in Experiment 1 (unit: mm)

esiduals in mm

#	Point	X	Y	Z
1	K2H	-0.1331	0.0701	-0.1043
2	C3H	0.0225	0.6917	0.1966
3	C3AH	0.0917	-0.0834	0.0012
4	CD3	0.0085	0.1034	-0.0499
5	C4H	0.2139	0.4431	0.0159
6	X11H	-0.1956	-0.1203	0.0424
7	X14H	-0.2707	-0.6789	0.0105
8	X21H	-0.1575	-0.6713	-0.0405
9	X23H	-0.2099	-0.4830	-0.0791
10	X24H	-0.3000	-0.8738	0.0487
11	X12H	-0.0833	0.0543	-0.0443
12	C5H	0.0965	0.9235	0.1370
13	L2H	-0.3839	-0.0760	-0.0299
14	CD6	0.2240	0.6469	0.0445
15	K3H	-0.2414	0.1681	-0.1923
16	D2H	-0.1741	-0.1351	0.1482
17	D4H	-0.3618	-0.5893	0.0837
18	DE3	0.0249	0.0972	0.0584
19	D5H	0.1103	-0.0200	0.0536
20	X41H	0.2417	0.2130	0.0163
21	X42H	-0.0036	0.3428	0.0442
22	X44H	0.2711	-0.1222	-0.0941
23	D7H	0.1875	-0.1979	0.1207
24	L3H	0.0363	0.4035	-0.0919
25	E3H	0.3612	0.3687	0.0231
26	K4H	-0.2794	-0.0702	-0.0482
27	EF3	0.3847	0.3115	-0.0655
28	E3AH	0.0301	-0.7128	-0.0224
29	F1H	0.0536	-0.8699	0.3925
30	J3H	-0.2177	-0.2311	-0.2388
31	F2H	-0.0073	-0.6748	0.1625
32	E4H	0.0773	0.0866	0.0348
33	EF4	-0.1400	0.0662	0.1251
34	EF5	0.0086	0.7368	0.0103
35	F3H	0.1351	0.6980	-0.1767
36	J5H	-0.2393	0.3747	-0.2765
37	E5H	0.0982	-0.1994	0.0408
38	EF6	-0.1276	-1.0336	0.1189
39	L4H	-0.1683	0.2552	-0.1671
40	F5H	0.1533	-0.1632	0.1039
41	J6H	-0.0388	0.6855	-0.5732
42	C4BH	0.2575	0.1718	-0.0087
43	D6H	0.1121	0.1600	0.0571
44	DE6	0.1454	-0.7418	0.1903
45	E4BH	0.2272	0.5950	0.0174
		0.1911	0.4820	0.1479

Total RMS = 0.5392 mm

This is the end of experiment.

The same experiment was carried out three times with similar configuration on different days. Only the final results for the other two experiments are shown on next two pages in order to indicate the repeatability of accuracy.

In the three sets of final result shown, only one point was filtered out because of its significantly larger residuals than the others. That was point L2H in experiment 2, whose residual in Y was 2.1646 mm, four times the average. The inconsistency of the total numbers of determined points for the three experiments was caused by mismatching, misidentification or absence of points.

It should be mentioned that the theodolite orientation in Experiment 2 was carried out by using the method of six-point relative orientation as introduced in Chapter 4. The six points were C4BH, EF6, J3H, K2H, L2H and X11H. The dual axial compensator was switched off in this case.

7.3 Result analysis

From the RMS of the residuals in X and Z in the final experiment results, it can be seen that the accuracy of determination in X and Z is consistently about 0.2 mm which is equivalent to 0.15 pixel in the image scale. This order of accuracy is within expectation because the target image location error alone is 0.1 pixel apart from the error contribution of calibration and configuration. The error in Y

Table 7-13 **Accuracy of the determined object coordinates in Experiment 2 (unit: mm)**

esiduals in mm

£	Point	X	Y	Z
1	K2H	-0.0129	-0.2835	-0.2575
2	K3H	-0.1621	0.1479	-0.3060
3	K4H	-0.2571	-0.2240	-0.1788
4	C3H	0.1841	-0.7782	0.1004
5	CD3	0.1886	-0.6068	-0.0706
6	C4H	0.3143	0.4694	0.2141
7	C5H	-0.1012	-0.1485	0.2353
8	CD6	0.0977	0.4266	0.2185
9	C3AH	0.3588	1.4840	0.3133
10	C4BH	-0.0042	-0.3519	0.0995
11	D3H	0.0422	0.3977	0.0407
12	DE3	-0.1975	-0.6149	0.0664
13	D5H	0.1327	0.7174	-0.0483
14	D6H	-0.1574	-0.2580	0.0031
15	D4H	0.1107	0.0844	0.1558
16	E3H	0.2232	0.0069	-0.0017
17	EF3	-0.0160	-0.4778	0.1012
18	E4H	0.0977	0.0273	0.0719
19	EF4	-0.1156	-0.0868	0.1673
20	E5H	0.1662	0.1916	0.0699
21	E3AH	0.2171	0.1678	-0.0775
22	E4BH	0.0565	0.5388	0.0492
23	EF6	-0.1734	-0.4841	0.1487
24	EF5	-0.2475	-0.1259	0.1619
25	F3H	-0.0462	0.1396	-0.1264
26	F5H	-0.0704	-1.0015	0.3871
27	F2H	-0.0847	-0.2639	-0.1167
28	F4H	-0.0762	-0.4510	0.1204
29	J3H	-0.1276	-0.4928	-0.2958
30	J4H	-0.2580	0.3279	-0.4141
31	J5H	-0.0709	0.2502	-0.4413
32	J6H	-0.2361	-0.0019	-0.3843
33	X12H	0.1722	0.7160	0.0972
34	X14H	-0.2135	-0.2796	0.0581
35	X21H	-0.0305	0.3641	0.0168
36	X23H	0.0605	0.2489	-0.0212
37	X41H	0.1920	0.0032	-0.0948
38	X42H	-0.2553	0.5358	-0.0556
39	X44H	0.0048	-0.1790	-0.0962
40	X11H	0.0326	-0.7902	0.0269
41	X24H	0.0661	0.0184	0.1770
42	L4H	0.2267	0.6347	-0.0890
		0.1644	0.4801	0.1871

Total RMS = 0.5409 mm

Table 7-14 **Accuracy of the determined object coordinates in Experiment 3 (unit: mm)**

esiduals in mm

t	Point	X	Y	Z
1	C3H	-0.0243	0.5156	0.1727
2	CD3	0.0508	0.0665	0.0817
3	C5H	-0.0539	-0.3907	0.1300
4	CD6	0.2609	0.7919	0.2074
5	C3AH	-0.2145	0.2268	0.1373
6	D3H	0.4485	0.0119	0.1392
7	DE3	-0.0008	0.1902	0.0293
8	D5H	-0.0077	-0.0228	0.0392
9	D7H	-0.0764	-0.9311	0.1456
10	DE6	0.3134	-0.2301	0.1920
11	E4H	0.1933	0.5612	-0.1704
12	E3H	0.2157	0.5497	-0.0218
13	EF3	0.1655	-0.1422	0.0543
14	E4H	-0.1867	0.5962	-0.0944
15	EF5	0.2577	0.2225	-0.0789
16	EF6	0.0801	0.3852	-0.0756
17	E5H	0.0995	0.1659	0.0037
18	E3AH	0.0883	-0.3561	0.0549
19	EF4	0.0457	0.1772	-0.0515
20	EF5	-0.1543	-0.9065	0.2451
21	EF6	0.0991	0.1392	-0.0966
22	F1H	0.1372	-0.6029	0.3140
23	F3H	0.1952	0.4318	-0.1826
24	F5H	-0.3485	-0.6538	0.2537
25	F2H	0.0650	-0.7043	0.1064
26	F4H	0.0153	-0.0175	-0.1169
27	J3H	-0.2166	0.2876	-0.3154
28	J4H	-0.3994	-0.5570	-0.1945
29	J6H	-0.1948	0.4984	-0.5011
30	J5H	-0.2958	-0.0054	-0.2096
31	K3H	-0.3019	-0.3411	-0.2765
32	K4H	-0.1344	-0.3760	-0.0058
33	X44H	0.0633	0.0197	-0.0208
34	X16H	-0.0770	-0.2125	0.0022
35	X21H	-0.1030	-0.9473	0.0061
36	L3H	0.0174	1.1645	0.1947
37	L4H	-0.0218	0.3954	-0.0972
		0.1905	0.4960	0.1725

Total RMS = 0.5587 mm

being over twice as large as that in X or Z is also within expectation for this particular base distance ratio of the configuration. The error in theodolite orientation should also contribute to the error in the three dimensional determination. In the experiments, however, this contribution is not shown significant as the orientation using either the reciprocal pointing method, five-point method or the method with many redundant points gave almost the same accuracy in the final results. This could be understood by considering the fact that 0.1 pixel image error and calibration error is equivalent to 10 seconds angular error for the camera used and that the accuracy of the theodolites is higher than 1 second.

It can easily be appreciated that if only one image had been taken on each of the two stations as in the conventional cases, only a third of the object could have been measured with the same accuracy. If the set-up of one image each station had been used to cover the whole object, a shorter focus lens or longer imaging distances would have had to be used and three time as great a root mean square error in object coordinates could have resulted. In terms of the measure of relative accuracy or the ratio of object RMS error to the largest dimension of the object, we can appreciate that with the mode of 3 × 3 theodolite scanning photogrammetry, the system can bring a three-fold improvement in this relative accuracy (or accuracy to size ratio).

These results of experiment have shown that theodolite scanning photogrammetry with theodolite-CCD cameras can effectively overcome the limitation of low resolution of

ordinary CCD cameras in three dimensional measurement and that the calibration and orientation methods used are effective.

Chapter 8. Conclusions

8.1 Conclusions

At the end of the research the following conclusions can be drawn:

CONCLUSION 1.
The novel control field free camera calibration method – the camera-on-theodolite method – proposed in this research is as effective as previous methods using control fields. It is particularly effective for calibrating theodolite-CCD cameras. It is also applicable to other cameras which can be rigidly mounted on the telescope of a theodolite.

The camera-on-theodolite calibration method is a contribution to the knowledge of analytical camera calibration in photogrammetry. It has significant characteristics in comparison to those methods written in photogrammetric books including the laboratory method, field method and stellar method (Slama, 1980 and Wolf, 1983).

The principle of the camera-on-theodolite method has been successfully used for the calibration of the narrow angle CCD camera in the motorized theodolite of the Leica SPACE system (Kyle, et al., 1990). It has also been used recently in a remote measuring system based on motorized theodolite-CCD cameras, which is still under development in the Department of Photogrammetry and Surveying, University College London (Chapman, et al., 1992). It is believed that the new method,

with its attractions, will be found more and more being used or adapted for camera calibration in its suitable cases in the future.

It is recommended that in order to promote the application of the new method for small film cameras, some easy to fix, detachable and universal mount be designed to mount the cameras on the telescopes of theodolites. The Wild P32 metric terrestrial cameras may gain more attractions if the current mount to the theodolites is modified into a more rigid one because the cameras can then be very precisely oriented by using the carrier theodolites and the camera-on-theodolite calibration method.

CONCLUSION 2.

The produced computer software for automatic CCD camera calibration using the camera-on-theodolite method is effective, efficient, easy to operate and ready for routine use for CCD calibration.

This software is part of the outcome of the project. It is also the important tool that has been used for many times in the experiments of the project. It is, therefore, well proved and believed to continue to be useful in future research involving theodolite-CCD cameras and in routine CCD camera calibration.

It should be mentioned that the geometry of a digital image is dependent of not only the CCD camera but also the image grabber used. What has been meant by CCD camera

calibration in the thesis as well as elsewhere is in fact the calibration of the digital image acquired using particular CCD cameras together with particular image grabbers. Hence, when in use for calibrating CCD cameras connected with image grabbers other than PCVISION plus, the software produced here inevitably needs some minor alteration relating the image capturing device. It is, however, straight forward.

CONCLUSION 3.

The algorithm designed and the program produced for automatic circular target image location are effective and of an accuracy as high as 0.02 pixel. This program can also be used for future projects where similar targets are used.

Automatic target image location is an important task of digital image processing for photogrammetry. It is involved in most of the research and application of digital and real-time photogrammetry. The accuracy achieved by the program produced in the project has matched the highest level of accuracy ever reported in the literature (Lenz, 1987 and Seitz, 1988).

It is experience worth mentioning that illumination condition greatly affect the accuracy of target image location and that scattered lighting is preferred to strongly directed lighting for a good accuracy in target image location. Glossy and reflective material should not be used for targets.

The accuracy of target image location in the sampling direction is normally worse than that in the line direction. This is mainly attributed to the linejitter. Measures as

introduced in Chapter 5 can be taken to correct for or reduce it in the future. It is recommended that the CCD cameras are set up with their sampling direction perpendicular to the base line so as to prevent the linejitter from contributing to the errors in x-parallaxes that determines the depth coordinate.

The running speed of the program was satisfactory for this project although it was out of the scope of this investigation. The program for correspondence of conjugate target images was working but some mismatch did occur. Improvement by using correlation algorithms is recommended for the future. Targets with artificial identification such as bar code may be adopted where possible to ensure correct correspondence as well as identification.

CONCLUSION 4.

The technique of theodolite scanning photogrammetry enables CCD cameras either to achieve better accuracy of object coordinate determination for a specified size of objects, or to measure larger objects with a specified accuracy than in the non-scanning case when only one image pair is taken with CCD cameras of the same characteristics.

This technique provides a solution to high accuracy digital photogrammetry using low cost CCD cameras. It forms an important function in the three dimensional measuring systems based on theodolite-CCD cameras.

8.2 Future work

This is the first part of the investigation of three dimensional measurement based on the combined theodolite-CCD cameras. Although the targeted fundamental problems have been successfully solved, many other problems are yet to be investigated before such theodolite-CCD camera systems become welcome by society as sensible tools for three dimensional measurement.

The immediate work needed to be done in the future is to reveal the accuracy potential of the system by experimenting with the theodolite scanning photogrammetry using longer focus lens. It is to be expected that the accuracy of three dimensional determination of theodolite scanning photogrammetry increases with the focal length of camera and so does the contribution of the theodolite orientation accuracy to the accuracy of three dimensional determination. Beyond some critical value of focal length, the theodolite orientation accuracy becomes the limiting factor where no accuracy gain can be made by further increasing the focal length. Accuracy can then only be improved by improving the theodolite orientation. To discover this critical value and the regularity of accuracy change with change of focal length is very interesting and important towards the development of a three dimensional measuring system based on theodolite-CCD cameras.

A great attraction of theodolite-CCD camera systems lies in automation with the help of motorized theodolites. As

envisaged at the beginning of the research, a measuring system based on motorized theodolite-CCD cameras has many more features over the current measuring systems. All those features can be developed in the future based on the outcome of the current research.

The most straight forward work recommended to be done when motorized theodolites are provided is to develop software to automate the whole processes of calibration and theodolite orientation and then the process of image capture for scanning photogrammetry. These form important features in a theodolite-CCD camera system and provide prerequisite conditions for further development of advanced functions including automatic target search and measuring while tracking.

Research and development in automatic functions of theodolite-CCD cameras inevitably involves very large expenditure. It is the author's hope that the outcome of this research can directly or indirectly do some good in attracting funding for future research in three dimensional measurement based on theodolite-CCD cameras.

Appendix: Camera Calibration Certificate

Camera Calibration Results

Job description

Camera: CCD made by Philips, 480 line*512 smaple *8 bits
Lens: TV lens made by Sony, 25 mm focal length,
Object distance: 4 metres
Apture: 2.0 f/D
Date: 22-05-1990 at UCL p&s
Operator: Yi Dong Huang
Calibration method: Camera-on-theodolite,
space resection with additional parameters

Error correction model:

$$x^* = xc + 100A*yc + 100000k1*xc*r2$$
$$y^* = yc + 100B*yc + 100000k1*yc*r2$$

where $xc = x1-x0$, $yc = y1-y0$, $r2 = xc*xc + yc*yc$

where $x1 = 0.7(x-240)$, $y1 = y-256$

where x^*, y^* denote the corrected line and sample respectively and
x, y " " original " " " .

Calibrated values:

Translations X,Y,Z mm:	.645	58.891	52.983
Rotations φ , ω , κ r radian:	.34480218E+00	.15583146E+01	-.19253052E+01
Principal distance f pixel(sample dir.):	2243.460		
Principal point x0(l),y0(s) pixel:	22.4908	46.2628	
AP(1-3) radia distortion k1,k2,k3:	.344E-12	.000E+00	.000E+00
AP(4-5) tangential dist. p1,p2:	.000E+00	.000E+00	
AP(8-9) affine deform. A,B :	-.674E-05	.379E-03	

AP(10-13,20)x:xy,yy,xxy,xyy,xx:

0.000000000000000E+000	0.000000000000000E+000	0.000000000000000E+000
0.000000000000000E+000	0.000000000000000E+000	

AP(14-19,21)y:x,y,xy,xx,xxy,xyy,yy:

0.000000000000000E+000	0.000000000000000E+000	0.000000000000000E+000
0.000000000000000E+000	0.000000000000000E+000	0.000000000000000E+000
0.000000000000000E+000		

P.T.O

Calibration accuracy (sample pixel):

Sigma0= .0525178 RMSX= .0322173 RMSY= .0586856

Standard errors of unkowns:

XO	YO	ZO	Φ	ω
.721261E-01	.937067E+00	.711718E-01	.327814E+03	.504612E+01
κ	f	x0	y0	k1
.327818E+03	.645520E+00	.484424E+01	.394421E+01	.319455E-13
A	B			
.125351E-05	.126691E-05			

Rotation matrix:

-.00973128	-.01170524	-.99988414
.99994375	-.00433266	-.00968114
-.00421883	-.99992210	.01174674

Image Coordinates &		Residuals (x,y,in sample pixel)	
1	-144.722	228.714	.053	.031
2	-70.857	204.154	.024	-.044
3	-4.834	204.586	.026	-.022
4	-11.694	229.517	-.002	.022
5	54.787	230.144	.018	-.039
6	129.537	205.755	-.043	.033
7	-138.680	104.879	-.044	.021
8	-72.590	105.391	-.014	.016
9	-79.009	131.044	-.012	-.042
10	-11.845	131.620	-.025	-.077
11	61.563	106.584	.044	-.022
12	128.893	107.256	.014	-.050
13	121.094	132.699	.005	.099
14	-145.037	28.546	-.013	-.047
15	-72.687	.858	-.007	.110
16	-4.728	1.576	-.029	.061
17	-11.631	27.930	-.036	-.014
18	54.100	28.479	-.039	.059
19	128.827	2.905	.030	-.004
20	-138.570	-104.460	-.019	-.117
21	-72.139	-103.806	-.036	.072
22	-78.643	-76.727	-.019	.092
23	-12.264	-75.932	-.014	.014
24	61.269	-102.262	.036	-.021
25	128.698	-101.582	.004	-.084
26	120.865	-74.617	.034	-.041
27	-145.245	-177.523	.061	-.103
28	-72.271	-204.609	.024	.005
29	-5.518	-203.814	.055	.065
30	-12.404	-175.942	-.026	.067
31	54.465	-175.160	.015	-.021
32	129.471	-202.352	-.064	-.037

RMSc= .047 RMSx= .032 RMSy= .059

Image Coordinates &		Residuals (x,y in pixel) for check points	
1	-138.806	203.773	.056	-.027
2	-77.284	229.121	.037	-.033
3	62.152	205.077	.015	.048
4	121.662	230.815	.000	-.024
5	-144.658	130.592	-.013	-.065
6	-4.981	106.119	.003	-.158
7	54.226	132.171	.030	-.034
8	-139.038	2.212	-.029	-.061
9	-79.095	27.230	-.044	.050
10	61.377	2.170	.038	.104
11	121.052	29.071	.005	.096
12	-144.616	-77.412	-.011	-.000
13	-5.344	-102.849	-.002	-.125
14	53.953	-75.193	-.015	-.072
15	-139.200	-205.636	.111	.023
16	-78.769	-176.592	-.012	-.101
17	61.852	-203.024	.025	.034
18	121.568	-174.602	.017	-.002

RMSc= .057 RMSx= .036 RMSy= .072

References

Abdel-Aziz, Y.I.and Karara, H.M., 1971, Direct transformation into object space coordinates in close-range photogrammetry. Symposium on Close-Range Photogrammetry, University of Illinois at Urbana-Champaign, Urbana, Illinois, January 26-29,1-18.

Beyer, H.A., 1987, Some aspects of the geometric calibration of CCD-cameras. Proceedings of the ISPRS inter-commission conference on "Fast processing of photogrammetric date". Interlaken, June 2-4, 68-81.

Bösemann, W., Godding, R. and Riechmann, W., 1990, Photogrammetric investigation of CCD cameras. Proceedings, ISPRS Commission V Symposium, Zürich, pp 119-126.

Brown, D.C., 1971 Close-range camera calibration, Photogrammetric Engineering. Vol. 37, No. 8, 855-866.

Chapman, D., Deacon, A. and Hamid, A., 1992. CAD modelling of radioactive plant: the role of digital photogrammetry in hazardous nuclear environments. Proceedings of the ISPRS Congress at Washington D.C. part B5, pp.741-753.

Curry, S.; Baumrind,S. and Anderson,J.M., 1986, Calibration of an array camera. Photogrammetric Engineering and Remote Sensing, 52(5).

Dähler, J., 1987. Problems in digital image acquisition with CCD-cameras. Proceedings of the ISPRS intercommission conference on "Fast processing of photogrammetric date". Interlaken, June 2-4,48-59.

El-Hakim, S.F. and Barakat, M.A., 1989, A vision-based coordinate measuring machine (VCCM). "Optical 3-D Measurement Techniques", Ed. Gruen/Kahmen, Wichmann.

Fraser, C.S. and Brown, D.C., 1986: Industrial photogrammetry-new developments and recent applications. The Photogrammetric Record 12.

Fritsch, D., 1989, Algorithms in fast vision system. "Optical 3-D measurement Techniques", Ed. Gruen/Kahmen, Wichmann.

Fryer, J.G. and Brown, D.C., 1986, Lens distortion for close-range photogrammetry. Photogrammetric Engineering and Remote Sensing, 52(1):51-58.

Gottwald, R., 1989, Kern E2-SE, a new instrument for industrial surveying. Kern Swiss Industrial Metrology

Gottwald, R., Berner, W., 1987: Electronic theodolite-sensor systems for real-time-photogrammetry? ISPRS Conference "Fast Processing of photogrammetric Date", Interlaken, June 2-4.

Haggrén, H., 1986: Real-time photogrammetry as used for machine vision applications. ISPRS Comm.V Symposium, Ottawa, pp.374-382.

Haggrén, H., 1987: Mapvision - the photogrammetric machine vision system. ISPRS Conference "Fast Processing of Photogrammetric Date", Interlaken, June 2-4.

Huang, Y.D. and Harley, I.A., 1989, Calibration of close-range photogrammetric stations using a free network bundle adjustment (sic), Optical 3-D measurement techniques (Editor A Gruen and H Kahmen). Wichmann, Karlsruh.495 pages: 49-56 (The correct title of the paper was A new camera calibration method needing no control field)

Huang, Y.D. and Harley, I.A., 1990, CCD camera calibration without a control field. ISPRS Commission V Symposium, Zürich, Sept. 3-7, 1990. pp 1028-1034

Huang, Y.D., 1992. 3-D measuring systems based on theodolite-CCD cameras. Proceedings of the ISPRS Congress at Washington D.C. part B5, pp 541-544.

Kyle, S.A., 1988. Triangulation methods in engineering measurement. Ph.D. thesis, University of London.

Kyle, S.A., Loser, R. and Rogers, J., 1990. Kern SPACE theodolite calibration. Proceedings, ISPRS Commission V Symposium, Zürich, pp.322-329.

Lenz, R.K., 1987, Lens distortion corrected CCD-camera calibration with co-planar calibration points for real time 3D measurements. Proceedings of the ISPRS intercommission conference on "Fast processing of photogrammetric data", Interlaken, June 2-4, pp 60-67.

Lenz, R. 1989, Image data acquisition with CCD cameras. "Optical 3-D Measurement Techniques", Edt. Gruen/Kahmen, Wichmann. pp 22-34.

Luhmann, T. and Wester-Ebbinghaus, W., 1987a: Digital image processing by means of reseau-scanning. The 41st Photogrammetric Week, Stuttgart.

Luhmann, T. and Wester-Ebbinghaus, W., 1987b: Image recording with opto-electronical matrix sensor - possibilities for on-line processing. Proceedings of the Second Industrial and Engineering Survey Conference, London.

Luhmann, T., 1990. Image recording system for close-range photogrammetry. Proceedings, ISPRS Commission V Symposium, Zürich, pp.86-95.

Macleod, A., Morris, J.R.W. and Lyster, M., 1990. Highly accurate video coordinate generation for automatic 3D trajectory calculation. Proceedings of the First World Congress of Biomedics. SPIE Vol 1356, pp.12-18.

Riechmann, W., 1988: Digital object recording by means of reseau-scanning. ISPRS Congress KYOTO, Commission V.

Schneider, C.-Th. and Sinnreich, K., 1990. Concept of an optical coordinate measurement machine. Proceedings, ISPRS Commission V Symposium, Zürich, pp.816-822.

Seitz, P., 1988, Optical superresolution using solid-state cameras and digital signal processing. Optical Engineering, 27 (7), pp 535-540.

Slama, C.C. (editor), 1980, Manual of photogrammetry. (4th edition), American Society of Photogrammetry.

Tsai, R.Y., 1985, A versatile camera calibration technique for high accuracy 3D machine vision metrology using off-the-shelf TV cameras and lenses. IBM Research Report RC 51342, May 8.

Wester-Ebbinghaus, W., 1988a. High resolution digital object recording by video-theodolites, ISPRS Congress Kyoto, Commission V, V219-V223.

Wester-Ebbinghaus, W., 1988b. Analytics in non-topographic photogrammetry. ISPRS Congress Kyoto, Invited Paper for Commission V.

Whittle, M. and Harris, D. (editors), 1985, Biomechanical Measurement in Orthopaedic Practice. Oxford University Press, Oxford.

Wolf, P.R., 1983. Elements of photogrammetry. (second edition) McGraw-Hill. 628 pages.